Strathprints Institutional Repository

Cowley, James and Mulholland, Anthony J. and Stewart, Iain W. and Gachagan, Anthony (2016) Mathematical modelling of the collapse time of an unfolding shelled microbubble. [Report] ,

This version is available at http://strathprints.strath.ac.uk/55869/

Mathematical Modelling of the Collapse Time of an Unfolding Shelled Microbubble

James Cowley[1], Anthony J. Mulholland[1], Iain W. Stewart[1] &

Anthony Gachagan[2]

[1]Department of Mathematics and Statistics,

University of Strathclyde,

26 Richmond Street,

Glasgow, G1 1XH.

[2]The Centre for Ultrasonic Engineering,

Department of Electronic and Electrical Engineering,

University of Strathclyde,

204 George Street,

Glasgow, G1 1XH.

Abstract

There is considerable interest at the moment on using shelled microbubbles as a transportation mechanism for localised drug delivery, specifically in the treatment of various cancers. In this report a theoretical model is

1

proposed which predicts the collapse time of an unfolding shelled microbubble. A neo-Hookean, compressible strain energy density function is used to model the potential energy per unit volume of the shell. This is achieved by considering a reference configuration (stress free) consisting of a shelled microsphere with a hemispherical cap removed. This is then displaced angularly and radially by applying a stress load to the free edge of the shell. This forms a deformed open sphere possessing a stress. This is then used as an initial condition to model the unfolding of the shell back to its original stress free configuration. Asymptotic expansion along with the conservation of mass and energy are then used to determine the collapse times for the unfolding shell and how the material parameters influence this. The theoretical model is compared to published experimental results.

1 Introduction

Ultrasound contrast agents (UCAs) are shelled microbubbles typically composed of a layer or numerous layers of a protein shell encapsulating a perfluoro gas which stabilises the shelled microbubble when it is injected into the bloodstream [1]. The shelled microbubbles have a typical radius of between 1 μm allowing them to propagate through the capillaries in the human body and a shell thickness that varies between 4 and 100 nm [2]. A typical shear modulus value for a monolipid UCA is $20MPa$ with a Poisson ratio of $\nu = 0.48$ [3, 4]. UCA's are currently licensed in the UK as ultrasound imaging contrast agents because they create a contrast with the surrounding tissue due to the production of seconday and higher harmonics. Microbubbles resonate with typical frequencies of 7 MHz producing nonlinear, multiple harmonic signals that enhance the quality of the medical imaging process [5]. The success of these shelled microbubbles as contrast agents has provided

impetus to their potential use as localised drug delivery agents. This procedure aims to minimise the pernicious side effects associated with current conventional chemotherapy treatments. Once the microbubbles are in the vicinity of the tumour the use of ultrasound chirps leads to acoustic microstreaming of the microbubbles near the endothelial cells that line the capillary wall. This results in the formation of cavitation bubbles that collapse rapidly to produce shock waves which create pores in the capillary walls [2]. The pores provide a doorway to the surface of the tumour where the chemical receptors guide the shelled microbubbles onto the surface of the tumour where they are burst by a high power, focussed ultrasound pulse. This bursting phase of the microbubble is obviously an important factor in the life cycle of this drug delivery mechanism and hence the use of theoretical modelling to deepen the understanding is critically important. In particular, the role that the material parameters of the shell, such as the thickness of the shell, its stiffness (shear modulus) and its Poisson ratio, have on the collapse time of the unfolding shell. The literature pertaining to the mathematical modelling of shelled microbubble collapse is very limited. Rayleigh's original work from 1917 contains an analytical solution for the collapse time of a ruptured shelled microbubble but it is valid only for a gas bubble (not shelled) in an inviscid liquid [6]. Müller performed a series of experiments on the rupture dynamics of smectic bubbles focussing on the velocity of the progressing rim around the growing rupture hole, the stability of the rim and the change in thickness of the film during the rupturing process [7]. Müller's work gives key experimental parameters and collapse times for a range of smectic shelled millibubble sizes and thicknesses that will be compared to the mathematical models that will be developed in this report. Bogoyavlenskiy's paper on the differential criterion of bubble collapse is an analytical approach that exploits the Rayleigh-Plesset equation specifically for a viscous,

Newtonian liquid [8]. This work derives a general collapse condition relating to the viscosity of the surrounding fluid but again it deals only with a gas bubble and not a shelled, viscoelastic microbubble. There currently exists very few studies in the literature pertaining specifically to UCA modelling using nonlinear elasticity which is, after all, the standard approach for modelling large deformations of elastic materials and in particular soft materials such as in biological settings [9]. There are some publications relating to the dynamics of spherical bodies using nonlinear elasticity [10] and a recent paper uses constitutive laws from nonlinear elasticity alongside the Kelvin-Voigt viscoelastic model to study the physical behaviour of various UCA types ranging from monolipids to polymers [9]. They suggest that the polymer based UCAs were consistent with the neo-Hookean model whereas monolipid UCAs were consistent with the Mooney-Rivlin constitutive law due to the presence of strain softening behaviour. Strain softening behaviour occurs due to the area density of the monolipid decreasing as the material stretches radially outwards. This behaviour has been observed in monolipids typically used in UCA shells such as Sonovue [11, 9].

2   Rupture of a shelled microbubble

In this section a theoretical model is proposed to predict the collapse time of an collapsing shell for a spherical, shelled microbubble. The same compressible, neo-Hookean [12] hyperelastic strain energy density function is used to model the potential energy per unit volume of the shell which is subjected to a stress via an opening angle [12]. The stress of the shell is generated by a sphere with a hole in

the south polar region; the open sphere represents the reference configuration. A series of polar hoop stress steps are applied to the ends of this open sphere resulting in the sphere experiencing both a radial and polar angular displacement. This stressed sphere then denotes the current configuration and possesses both radial and hoop stresses which are evaluated using the hyperelastic strain energy density function in conjunction with the relevant boundary conditions and the momentum balance law. The application of the polar hoop stresses to deform the sphere is done via a quasistatic process and so is thus independent of time resulting in a momentum balance equation that is equal to zero. The radial stresses at both the inner and outer radii of the compressible shell are set to zero during the quasistatic deformation procedure. An opening angle $\pi - \Theta_{op}$ is chosen that is small compared to π thus enabling the use of an asymptotic expansion approach (see Figure 1).
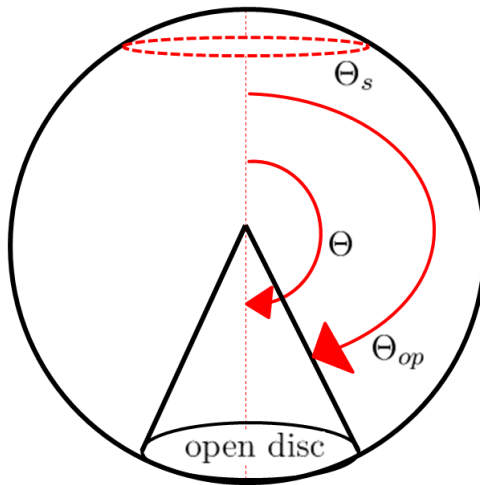

Figure 1: Figure illustrating the opening angle, $\pi - \Theta_{op}$, and the matching boundary condition, Θ_s, for a shelled microsphere.

The spatial profiles of the Cauchy radial and angular hoop stresses that are created within the shell during the quasistatic process are determined using the technique of linearisation alongside the momentum balance law and the conserva-

tion of mass. Since the shell is modelled as compressible this results in a change in volume and thickness of the shell for the stressed shell. The change in thickness of the shell is described using the Jacobian of the shell which illustrates both a radial and an angular dependency. This angular dependency results in coordinate singularites at the north and south poles of the sphere. To overcome the coordinate singularity, a small region (typically of the order of 1% of π) is reserved at the North pole, where the Jacobian is approximated as being purely radially dependent and hence exhibits no angular dependency. A matching boundary condition is then used to model the two regions; one region which is purely radially dependent and compressible and a much larger region which has both a radial and angular dependency and is also compressible in nature. The deformation used to link the reference configuration to the current configuration has both an angular and a radial dependency and so produces two differential equations; one describing the polar angle and the other the radial direction. This necessitates the requirement for two different sets of boundary conditions, one set for the polar angle and the other set for the radial behaviour. The process of deforming an open shelled spherical microbubble will be referred to as the forward picture where the forward picture's physical path will be utilised as an initial condition to determine the subsequent collapse phase of the collapsed shell.

Once the sphere has been stressed a change in the boundary conditions around the rim of the opening in the sphere is used to collapse the stressed sphere. To collapse the shell the hoop stress load is set to zero (this can be thought of as sticking a pin in a balloon). Switching off the stress load causes the stressed shell to collapse back down to its original, open, deformed location resulting in its original stress free, reference configuration. This collapse process is evaluated by resolving the radial

6

and angular stresses that act on the shell, taking into account their appropriate directions, and by applyingthe momentum equation alongside the new polar, hoop stress boundary conditions. It is assumed that in switching off the stress load at the opening angle that there is no external impulse adding to or subtracting from the initial potential energy per unit volume of the shell. This means that the collapse path will match the forward picture and since there is no viscosity or viscoelastic behaviour in our physical model then there will be no hysteresis. The physical behaviour of the collapsing shell will be typical of an oscillating helical spring exhibiting simple harmonic motion where the collapse time is dependent on the physical properties and characteristics of the material's shell. Results are produced from the model to show the influence of the shell's thickness, its Poisson ratio and the shear modulus on the collapse times of the collapsing shell.

3   Calculating the deformation for the forward picture

In this section a model will be developed to determine the Cauchy radial and angular (hoop) stresses in a deformed, open shelled microbubble when it is subjected to both an angular and a radial deformation. Let us consider the reference configuration of a stress free shell where a configuration of a body is defined as a one-to-one correspondence that maps the particles of the body onto their locations in Euclidean space ([13],p77). The reference configuration in cartesian coordinates is defined as (X^1, X^2, X^3) and is more generally denoted as X^i whereas the current configuration, representing the stressed sphere, is defined using the cartesian coordinates (x^1, x^2, x^3) which can be generalised to x^i. The stress free, open shell has an inner and outer radii described by R_I and R_O respectively whilst the deformed

7

stressed shell has an inner and outer radii denoted by $r(R_I)$ and $r(R_O)$. A radial deformation acting on the stress free, open sphere, is represented by

$$\chi = r(R, \Theta)e_r, \tag{1}$$

such that the polar angle in the current configuration is a function of the polar angle in the reference configuration and is expressed by $\theta = \theta(\Theta)$ and e_r represents the standard basis spherical polar coordinates ([13],p66). We will use a mixed tensorial basis and define the deformation gradient as $F = \nabla \otimes \chi$ ([13],p83-84); that is

$$F = \left(\frac{\partial \chi_i}{\partial X^j} + \chi_n \frac{\partial g^n}{\partial X^j} \cdot g_i \right) g^i \otimes G^j. \tag{2}$$

In spherical polar coordinates the current configuration is transformed into physical components ([13],p64) yielding $\chi_1 = \chi_r$, $\chi_2 = ru_\theta$ and $\chi_3 = r\sin\theta\chi_\phi$ where the physical coordinates preserve the units. Using equation (2) we can determine the gradient of the deformation defined by equation (1) where $\chi_1 = r(R, \Theta)$ and $\chi_2 = \chi_3 = 0$. For the opening angle approach $\theta = \theta(\Theta)$ and $\phi = \Phi$ resulting in a deformation, F, that is given by

$$
\begin{aligned}
(\nabla \otimes \chi)_{11} &= \left(\frac{\partial \chi_1}{\partial X^1} + \chi_1 \frac{\partial g^1}{\partial X^1} \cdot g_1 \right) g^1 \otimes G^1, \\
&= \left(\frac{\partial r}{\partial R} + r \frac{\partial e_r}{\partial R} \cdot e_r \right) e_r \otimes e_R, \\
&= \left(\frac{\partial r}{\partial R} \right) e_r \otimes e_R,
\end{aligned}
\tag{3}
$$

8

$$(\nabla \otimes \chi)_{12} = \left(\frac{\partial \chi_1}{\partial X^2} + \chi_1 \frac{\partial g^1}{\partial X^2} \cdot g_1 \right) g^1 \otimes G^2,$$

$$= \left(\frac{\partial r}{\partial \Theta} + r \frac{\partial e_r}{\partial \Theta} \cdot e_r \right) \frac{e_r \otimes e_\Theta}{R},$$

$$= \frac{1}{R} \left(\frac{\partial r}{\partial \Theta} \right) e_r \otimes e_\Theta, \tag{4}$$

$$(\nabla \otimes \chi)_{13} = \left(\frac{\partial \chi_1}{\partial X^3} + \chi_1 \frac{\partial g^1}{\partial X^3} \cdot g_1 \right) g^1 \otimes G^3,$$

$$= \left(r \frac{\partial e_r}{\partial \Phi} \cdot e_r \right) \frac{e_r \otimes e_\Phi}{R \sin \Phi},$$

$$= \left(r \sin \theta e_\phi \phi' \cdot e_r \right) \frac{e_r \otimes e_\Phi}{R \sin \Theta} = 0, \tag{5}$$

$$(\nabla \otimes \chi)_{21} = \left(\frac{\partial \chi_2}{\partial X^1} + \chi_1 \frac{\partial g^1}{\partial X^1} \cdot g_2 \right) g^2 \otimes G^1,$$

$$= \left(r \frac{\partial e_r}{\partial R} \cdot r e_\theta \right) \frac{e_\theta \otimes e_R}{r} = 0, \tag{6}$$

$$(\nabla \otimes \chi)_{22} = \left(\frac{\partial \chi_2}{\partial X^2} + \chi_1 \frac{\partial g^1}{\partial X^2} \cdot g_2 \right) g^2 \otimes G^2,$$

$$= \frac{r}{R} \left(e_\theta \frac{\partial \theta}{\partial \Theta} \cdot e_\theta \right) e_\theta \otimes e_\Theta = \frac{r}{R} \left(\frac{\partial \theta}{\partial \Theta} \right) e_\theta \otimes e_\Theta, \tag{7}$$

$$(\nabla \otimes \chi)_{23} = \left(\frac{\partial \chi_2}{\partial X^3} + \chi_1 \frac{\partial g^1}{\partial X^3} \cdot g_2 \right) g^2 \otimes G^3,$$

$$= \left(r \frac{\partial e_r}{\partial \Phi} \cdot r e_\theta \right) \frac{e_\theta \otimes e_\Phi}{r R \sin \Theta} = 0, \tag{8}$$

9

$$(\nabla \otimes \chi)_{31} = \left(\frac{\partial \chi_3}{\partial X^1} + \chi_1 \frac{\partial g^1}{\partial X^1} \cdot g_3 \right) g^3 \otimes G^1,$$

$$= \left(r \frac{\partial e_r}{\partial R} \cdot r \sin \theta e_\phi \right) \frac{e_\phi \otimes e_R}{r \sin \theta} = 0, \qquad (9)$$

$$(\nabla \otimes \chi)_{32} = \left(\frac{\partial \chi_3}{\partial X^2} + \chi_1 \frac{\partial g^1}{\partial X^2} \cdot g_3 \right) g^3 \otimes G^2,$$

$$= \left(r e_\theta \frac{\partial \theta}{\partial \Theta} \cdot r \sin \theta e_\phi \right) \frac{e_\phi \otimes e_\Theta}{r R \sin \theta} = 0, \qquad (10)$$

and

$$(\nabla \otimes \chi)_{33} = \left(\frac{\partial \chi_3}{\partial X^3} + \chi_1 \frac{\partial g^1}{\partial X^3} \cdot g_3 \right) g^3 \otimes G^3,$$

$$= \left(r \frac{\partial e_r}{\partial \Phi} \cdot r \sin \theta e_\phi \right) \frac{e_\phi \otimes e_\Phi}{r R \sin \theta \sin \Theta},$$

$$= \left(\frac{r \sin \theta}{R \sin \Theta} \right) e_\phi \otimes e_\Phi. \qquad (11)$$

Combining equations (3) - (11) and writing them as a 3×3 matrix since the gradient of the deformation written as $F = \nabla \otimes \chi$ is a two point tensor, gives

$$F = \begin{pmatrix} \frac{\partial r}{\partial R} & \frac{1}{R} \frac{\partial r}{\partial \Theta} & 0 \\ 0 & \frac{r}{R} \left(\frac{\partial \theta}{\partial \Theta} \right) & 0 \\ 0 & 0 & \frac{r \sin \theta}{R \sin \Theta} \end{pmatrix}. \qquad (12)$$

with an inverse transpose, F^{-T}, given by

$$F^{-T} = \begin{pmatrix} \frac{\partial R}{\partial r} & 0 & 0 \\ -\frac{1}{r} \left(\frac{\partial R}{\partial r} \right) \left(\frac{\partial r}{\partial \Theta} \right) \frac{\partial \Theta}{\partial \theta} & \frac{R}{r} \left(\frac{\partial \Theta}{\partial \theta} \right) & 0 \\ 0 & 0 & \frac{R \sin \Theta}{r \sin \theta} \end{pmatrix}. \qquad (13)$$

10

4 Hyperelastic strain energy density function

In this section the First Piola Kirchoff stress tensor will be derived for a neo-Hookean, compressible strain energy density function. Let us assume that the shell's material is hyperelastic so that there exists a strain energy density function (expressing the potential energy per unit volume), that is neo-Hookean [14, 12, 15], $W(F)$, and let it include a compressible term that is used to model the change in volume of the shell as it is stressed. The determinant of F, gives a measure of how the volume of the spherical shell changes as it maps from the stress free, reference configuration to the stressed, current configuration. The Jacobian (determinant of F) is therefore

$$J = \frac{r^2}{R^2} \left(\frac{\partial r}{\partial R} \right) \left(\frac{\partial \theta}{\partial \Theta} \right) \frac{\sin \theta}{\sin \Theta}. \tag{14}$$

The neo-Hookean strain energy density function is ([12], equation(5)) given by equation (**??**). The stresses can be described using the first Piola-Kirchhoff stress tensor which is the transpose of the nominal stress tensor, expressing the force in the current configuration in terms of the area in the reference configuration [12]. The Cauchy stresses relate the force in the current configuration to the area in the current configuration. The first Piola-Kirchhoff stress tensor, $S(F)$, is calculated using the following trace properties $\partial J/\partial F = JF^{-T}$ and $\partial(\mathrm{tr}(FF^T))/\partial F = 2F$, resulting in ([12], equation(5))

$$S(F) = \frac{\partial W}{\partial F} = \frac{\mu}{2}(2F) + \frac{\mu}{2\beta}\left(-2\beta J^{-2\beta-1}\frac{\partial J}{\partial F}\right),$$
$$= \mu\left(-J^{-2\beta}F^{-T} + F\right). \tag{15}$$

Substituting equations (12) and (13) into equation (15) leads to

$$S = S_{rR}e_r \otimes e_R + S_{\theta\Theta}e_\theta \otimes e_\Theta + S_{\phi\Phi}e_\phi \otimes e_\Phi + S_{r\Theta}e_r \otimes e_\Theta + S_{\theta R}e_\theta \otimes e_R,$$

$$= \mu\left(-J^{-2\beta}\frac{\partial R}{\partial r} + \frac{\partial r}{\partial R}\right)e_r \otimes e_R + \mu\left(-J^{-2\beta}\frac{R}{r}\left(\frac{\partial\Theta}{\partial\theta}\right) + \frac{r}{R}\left(\frac{\partial\theta}{\partial\Theta}\right)\right)e_\theta \otimes e_\Theta$$

$$+ \mu\left(-J^{-2\beta}\frac{R\sin\Theta}{r\sin\theta} + \frac{r\sin\theta}{R\sin\Theta}\right)e_\phi \otimes e_\Phi + \frac{\mu}{R}\left(\frac{\partial r}{\partial\Theta}\right)e_r \otimes e_\Theta$$

$$+ \frac{\mu J^{-2\beta}}{r}\left(\frac{\partial R}{\partial r}\right)\left(\frac{\partial r}{\partial\Theta}\right)\frac{\partial\Theta}{\partial\theta}e_\theta \otimes e_R. \quad (16)$$

Note that equation (16) identifies the physical components for $S_{rR}, S_{\theta\Theta}, S_{\phi\Phi}$ etc.

5 Calculating the divergence of the First Piola Kirchoff stress tensor for the forward picture

In this section the divergence of the First Piola Kirchoff stress tensor is derived for the stressing of shelled microbubble. The open, stress free sphere is deformed by applying a series of stresses directed towards the pole and applied on the rim of the open surface at the opening angle. Each one of which is modelled as a quasistatic deformation (1); the momentum is zero. This implies that the divergence of the first Piola Kirchoff stress tensor must satisfy $\nabla \cdot S = 0$. We need to be able to relate the physical coordinates for the mixed tensorial basis to the general basis vectors represented by the components g_i and G_i where $i \in \{1, 2, 3\}$. The first Piola-Kirchhoff stress tensor is represented by ([13],p34), $S = S_i^j g^i \otimes G_j$ where S_i^j are the left-covariant components of S. Converting into physical coordinates using equation (16) yields

$$S_1^1 g^1 \otimes G_1 = S_1^1 e_r \otimes e_R = S_{rR}e_r \otimes e_R,$$

where

$$S_1^1 = S_{rR} = \mu \left(-J^{-2\beta} \frac{\partial R}{\partial r} + \frac{\partial r}{\partial R} \right), \tag{17}$$

and

$$S_2^2 g^2 \otimes G_2 = S_2^2 \left(\frac{R}{r} \right) e_\theta \otimes e_\Theta = S_{\theta\Theta} e_\theta \otimes e_\Theta,$$

thus

$$S_2^2 = \mu \left(-J^{-2\beta} \left(\frac{\partial \Theta}{\partial \theta} \right) + \frac{r^2}{R^2} \left(\frac{\partial \theta}{\partial \Theta} \right) \right), \tag{18}$$

and

$$S_3^3 g^3 \otimes G_3 = S_3^3 \left(\frac{R \sin \Theta}{r \sin \theta} \right) e_\phi \otimes e_\Phi = S_{\phi\Phi} e_\phi \otimes e_\Phi,$$

resulting in

$$S_3^3 = \mu \left(-J^{-2\beta} + \left(\frac{r \sin \theta}{R \sin \Theta} \right)^2 \right). \tag{19}$$

Similarly

$$S_1^2 g^1 \otimes G_2 = S_1^2 e_r \otimes R e_\Theta = S_{r\Theta} e_r \otimes e_\Theta,$$

where

$$S_1^2 = \frac{\mu}{R^2} \left(\frac{\partial r}{\partial \Theta} \right), \tag{20}$$

and

$$S_2^1 g^2 \otimes G_1 = S_2^1 \frac{e_\theta}{r} \otimes e_R = S_{\theta R} e_\theta \otimes e_R,$$

resulting in

$$S_2^1 = \mu J^{-2\beta} \left(\frac{\partial R}{\partial r} \right) \left(\frac{\partial r}{\partial \Theta} \right) \frac{\partial \Theta}{\partial \theta}. \tag{21}$$

13

Calculating the divergence of S where

$$\nabla \cdot S = \frac{\partial}{\partial X^k} \left(S_i^{\;j} g^i \otimes G_j \right) \cdot G^k, \tag{22}$$

leads to

$$\frac{\partial}{\partial X^1} \left(S_1^{\;1} g^1 \otimes G_1 \right) \cdot G^1 = \frac{\partial S_1^{\;1}}{\partial R} \left(e_r \otimes e_R \right) \cdot e_R = \frac{\partial S_1^{\;1}}{\partial R} e_r. \tag{23}$$

Similarly we get

$$\begin{aligned}
\frac{\partial}{\partial X^1} \left(S_2^{\;2} g^2 \otimes G_2 \right) \cdot G^1 &= \frac{\partial}{\partial R} \left(S_2^{\;2} \frac{e_\theta}{r} \otimes R e_\Theta \right) \cdot e_R, \\
&= \frac{\partial}{\partial R} \left(S_2^{\;2} \frac{R}{r} \right) \left(e_\theta \otimes e_\Theta \right) \cdot e_R = 0, \tag{24}
\end{aligned}$$

since $(e_\theta \otimes e_\Theta) \cdot e_R = 0$ and both e_θ and e_Θ have no R dependency. Similarly

$$\begin{aligned}
\frac{\partial}{\partial X^1} \left(S_3^{\;3} g^3 \otimes G_3 \right) \cdot G^1 &= \frac{\partial}{\partial R} \left(S_3^{\;3} \frac{e_\phi}{r \sin \theta} \otimes R \sin \Theta e_\Phi \right) \cdot e_R, \\
&= \frac{\partial}{\partial R} \left(S_3^{\;3} \frac{R \sin \Theta}{r \sin \theta} \right) \left(e_\phi \otimes e_\Phi \right) \cdot e_R = 0. \tag{25}
\end{aligned}$$

The off diagonal terms are

$$\frac{\partial}{\partial X^1} \left(S_1^{\;2} g^1 \otimes G_2 \right) \cdot G^1 = 0, \tag{26}$$

and

$$\frac{\partial}{\partial X^1} \left(S_2^{\;1} g^2 \otimes G_1 \right) \cdot G^1 = \left(\frac{\partial S_2^{\;1}}{\partial R} \right) \frac{e_\theta}{r} - \frac{S_2^{\;1}}{r^2} \left(\frac{\partial r}{\partial R} \right) e_\theta. \tag{27}$$

14

Other terms are

$$\frac{\partial}{\partial X^2}\left(S_1^{\,1}g^1 \otimes G_1\right) \cdot G^2 = \frac{S_1^{\,1}}{R}\left(e_r \otimes e_\Theta\right) \cdot e_\Theta,$$

$$= \frac{S_1^{\,1}}{R}\left(e_r \otimes e_\Theta\right) \cdot e_\Theta = \frac{S_1^{\,1}}{R}e_r, \qquad (28)$$

also

$$\frac{\partial}{\partial X^2}\left(S_2^{\,2}g^2 \otimes G_2\right) \cdot G^2 = \frac{\partial S_2^{\,2}}{\partial \Theta}\left(\frac{e_\theta}{r}\right) + S_2^{\,2}\frac{\partial}{\partial \Theta}\left(\frac{e_\Theta}{r}\right),$$

$$= \frac{\partial S_2^{\,2}}{\partial \Theta}\left(\frac{e_\theta}{r}\right) - \frac{S_2^{\,2}}{r^2}\left(\frac{\partial r}{\partial \Theta}\right)e_\theta - \frac{S_2^{\,2}}{r}\left(\frac{\partial \theta}{\partial \Theta}\right)e_r, \qquad (29)$$

similarly

$$\frac{\partial}{\partial X^2}\left(S_3^{\,3}g^3 \otimes G_3\right) \cdot G^2 = \left(S_3^{\,3}\frac{e_\phi}{r \sin \theta} \otimes \frac{\partial}{\partial \Theta}\left(R \sin \Theta e_\Phi\right)\right) \cdot \frac{e_\Theta}{R} = 0, \qquad (30)$$

and

$$\frac{\partial}{\partial X^2}\left(S_1^{\,2}g^1 \otimes G_2\right) \cdot G^2 = \frac{\partial S_1^{\,2}}{\partial X^2}g^1 + S_1^{\,2}\frac{\partial g^1}{\partial X^2} + S_1^{\,2}g^1 \otimes \frac{\partial}{\partial \Theta}\left(Re_\Theta\right) \cdot G^2,$$

$$= \frac{\partial S_1^{\,2}}{\partial \Theta}e_r + S_1^{\,2}\left(\frac{\partial \theta}{\partial \Theta}\right)e_\theta, \qquad (31)$$

and

$$\frac{\partial}{\partial X^2}\left(S_2^{\,1}g^2 \otimes G_1\right) \cdot G^2 = \left(S_2^{\,1}g^2 \otimes \frac{\partial G_1}{\partial X^2}\right) \cdot G^2,$$

$$= \left(S_2^{\,1}\frac{e_\theta}{r} \otimes \frac{\partial}{\partial \Theta}e_R\right) \cdot \frac{e_\Theta}{R} = \frac{S_2^{\,1}}{Rr}e_\theta. \qquad (32)$$

15

Other components are

$$\frac{\partial}{\partial X^3}\left(S_1^{\ 1}g^1\otimes G_1\right)\cdot G^3=\left(S_1^{\ 1}g^1\otimes\frac{\partial e_R}{\partial\Phi}\right)\cdot G^3,$$

$$=\left(S_1^{\ 1}e_r\otimes\sin\Theta e_\Phi\right)\cdot\frac{e_\Phi}{R\sin\Theta}=\frac{S_1^{\ 1}}{R}e_r, \qquad (33)$$

and

$$\frac{\partial}{\partial X^3}\left(S_2^{\ 2}g^2\otimes G_2\right)\cdot G^3=S_2^{\ 2}\frac{e_\theta}{r}\otimes\frac{\partial}{\partial\Phi}\left(Re_\Phi\right)\cdot\frac{e_\Phi}{R\sin\Theta},$$

$$=S_2^{\ 2}\frac{e_\theta}{r}\otimes R\cos\Theta e_\Phi\cdot\frac{e_\Phi}{R\sin\Theta}=\frac{S_2^{\ 2}\cot\Theta}{r}e_\theta, \qquad (34)$$

also

$$\frac{\partial}{\partial X^3}\left(S_3^{\ 3}g^3\otimes G_3\right)\cdot G^3=S_3^{\ 3}\frac{\partial}{\partial\Phi}\left(\frac{e_\phi}{r\sin\theta}\right),$$

$$=-\frac{S_3^{\ 3}}{r}e_r-\frac{S_3^{\ 3}\cot\theta}{r}e_\theta, \qquad (35)$$

similarly

$$\frac{\partial}{\partial X^3}\left(S_1^{\ 2}g^1\otimes G_2\right)\cdot G^3=S_1^{\ 2}e_r\otimes\frac{\partial}{\partial\Phi}\left(Re_\Theta\right)\cdot\frac{e_\Phi}{R\sin\Theta},$$

$$=S_1^{\ 2}e_r\otimes\cos\Theta e_\Phi\cdot\frac{e_\Phi}{\sin\Theta}=\cot\Theta S_1^{\ 2}e_r, \qquad (36)$$

and

$$\frac{\partial}{\partial X^3}\left(S_2^{\ 1}g^2\otimes G_1\right)\cdot G^3=S_2^{\ 1}g^2\otimes\frac{\partial G_1}{\partial X^3}\cdot G^3,$$

$$=S_2^{\ 1}\frac{e_\theta}{r}\otimes\frac{\partial e_R}{\partial\Phi}\cdot\frac{e_\Phi}{R\sin\Theta}=\frac{S_2^{\ 1}}{rR}e_\theta. \qquad (37)$$

6   Radial and angular equations

In this section, the radial and angular equations are derived for a stressed shelled microbubble. Combining equations (23) to (37) and substituting into equation (22) results in the following radial and angular equations respectively

$$\frac{\partial S_1^1}{\partial R} + \frac{2S_1^1}{R} - \frac{S_2^2}{r}\left(\frac{\partial \theta}{\partial \Theta}\right) - \frac{S_3^3}{r} + \frac{\partial S_1^2}{\partial \Theta} + \cot \Theta S_1^2 = 0, \tag{38}$$

and,

$$\frac{1}{r}\left(\frac{\partial S_2^1}{\partial R}\right) - \frac{S_2^1}{r^2}\left(\frac{\partial r}{\partial R}\right) + \frac{1}{r}\left(\frac{\partial S_2^2}{\partial \Theta}\right) - \frac{S_2^2}{r^2}\left(\frac{\partial r}{\partial \Theta}\right)$$
$$+ S_1^2\left(\frac{\partial \theta}{\partial \Theta}\right) + \frac{2S_2^1}{Rr} + \frac{S_2^2 \cot \Theta}{r} - \frac{S_3^3 \cot \theta}{r} = 0. \tag{39}$$

Note that equations (38) and (39) represent the nondimensionalised stresses in a mixed tensorial basis and are the transpose of the nominal stresses. The first Piola Kirchoff tensor is related to the Cauchy stress tensor via

$$\tau = \frac{1}{J}\left(SF^T\right), \tag{40}$$

where J, the Jacobian, is given by equation (14) and F is described by equation (12) [12]. Using equation (40) in conjunction with equations (17) to (21), alongside equations (12) and (40) result in Cauchy stress terms that are given by the following expressions

$$\tau_{rr} = \frac{1}{J}\left(S_{rR}\frac{\partial r}{\partial R} + \frac{S_{r\Theta}}{R}\left(\frac{\partial r}{\partial \Theta}\right)\right),$$
$$= \frac{\mu}{J}\left(-J^{-2\beta} + \left(\frac{\partial r}{\partial R}\right)^2 + \frac{1}{R^2}\left(\frac{\partial r}{\partial \Theta}\right)^2\right), \tag{41}$$

alongside

$$\tau_{\theta\theta} = \frac{1}{J}\left(S_{\theta\Theta}\left(\frac{r}{R}\right)\frac{\partial\theta}{\partial\Theta}\right),$$
$$= \frac{\mu}{J}\left(-J^{-2\beta} + \left(\frac{r}{R}\right)^2\left(\frac{\partial\theta}{\partial\Theta}\right)^2\right), \tag{42}$$

and

$$\tau_{\phi\phi} = \frac{S_{\phi\Phi}}{J}\left(\frac{r\sin\theta}{R\sin\Theta}\right) = \frac{\mu}{J}\left(-J^{-2\beta} + \left(\frac{r\sin\theta}{R\sin\Theta}\right)^2\right). \tag{43}$$

The off diagonal term is given by

$$\tau_{r\theta} = \frac{1}{J}\left(S_{r\Theta}\right)\frac{r}{R}\left(\frac{\partial\theta}{\partial\Theta}\right) = \frac{\mu r}{JR^2}\left(\frac{\partial\theta}{\partial\Theta}\right)\frac{\partial r}{\partial\Theta}. \tag{44}$$

The radial equation can be written in terms of $r(R,\Theta)$ and $\theta(\Theta)$ by substituting equations (17) to (21) into equation (38) where,

$$\frac{\partial J}{\partial R} = J\left(\frac{2}{r}\left(\frac{\partial r}{\partial R}\right) + \left(\frac{\partial R}{\partial r}\right)\frac{\partial^2 r}{\partial R^2} - \frac{2}{R}\right), \tag{45}$$

and

$$\frac{\partial S_1^1}{\partial R} = \mu\left(\frac{\partial^2 r}{\partial R^2}\left(1 + (2\beta+1)J^{-2\beta}\left(\frac{\partial R}{\partial r}\right)^2\right) + J^{-2\beta}\left(\frac{4\beta}{r} - \frac{4\beta}{R}\left(\frac{\partial R}{\partial r}\right)\right)\right), \tag{46}$$

similarly

$$\frac{2S_1^1}{R} = \mu\left(\frac{-2J^{-2\beta}}{R}\left(\frac{\partial R}{\partial r}\right) + \frac{2}{R}\left(\frac{\partial r}{\partial R}\right)\right), \tag{47}$$

also

$$-\frac{S_2^2}{r}\left(\frac{\partial\theta}{\partial\Theta}\right) = \mu\left(\frac{J^{-2\beta}}{r} - \frac{r}{R^2}\left(\frac{\partial\theta}{\partial\Theta}\right)^2\right), \tag{48}$$

18

and

$$-\frac{S_3{}^3}{r} = \mu \left(\frac{J^{-2\beta}}{r} - \frac{r\sin^2\theta}{R^2\sin^2\Theta} \right). \tag{49}$$

The off diagonal terms are

$$\frac{\partial S_1{}^2}{\partial\Theta} = \frac{\mu}{R^2}\left(\frac{\partial^2 r}{\partial\Theta^2} \right), \tag{50}$$

and

$$\cot\Theta S_1{}^2 = \frac{\mu\cot\Theta}{R^2}\left(\frac{\partial r}{\partial\Theta} \right). \tag{51}$$

Substituting equations (46) to (51) into equation (38) yields

$$\frac{\partial^2 r}{\partial R^2}\left(1 + (2\beta+1)J^{-2\beta}\left(\frac{\partial R}{\partial r}\right)^2 \right) + J^{-2\beta}\left(\frac{4\beta}{r} - \frac{4\beta}{R}\left(\frac{\partial R}{\partial r}\right) - \frac{2}{R}\left(\frac{\partial R}{\partial r}\right) + \frac{2}{r} \right)$$
$$+ \frac{2}{R}\left(\frac{\partial r}{\partial R}\right) - \frac{r}{R^2}\left(\frac{\partial\theta}{\partial\Theta}\right)^2 - \frac{r\sin^2\theta}{R^2\sin^2\Theta} + \frac{1}{R^2}\left(\frac{\partial^2 r}{\partial\Theta^2}\right) + \frac{\cot\Theta}{R^2}\left(\frac{\partial r}{\partial\Theta}\right) = 0. \tag{52}$$

For the angular equation given by equation (39), the following is required

$$\frac{\partial J}{\partial\Theta} = \frac{\partial}{\partial\Theta}\left(\frac{r^2}{R^2}\left(\frac{\partial r}{\partial R}\right)\left(\frac{\partial\theta}{\partial\Theta}\right)\frac{\sin\theta}{\sin\Theta} \right),$$
$$= J\left(\frac{2}{r}\frac{\partial r}{\partial\Theta} + \left(\frac{\partial R}{\partial r}\right)\frac{\partial^2 r}{\partial\Theta\partial R} + \frac{\partial^2\theta}{\partial\Theta^2}\left(\frac{\partial\Theta}{\partial\theta}\right) + \frac{\partial\theta}{\partial\Theta}\cot\theta - \cot\Theta \right), \tag{53}$$

and

$$\frac{1}{r}\frac{\partial S_2{}^2}{\partial\Theta} = \mu\left(J^{-2\beta}\left(\frac{4\beta}{r^2}\left(\frac{\partial\Theta}{\partial\theta}\right)\left(\frac{\partial r}{\partial\Theta}\right) + \frac{2\beta}{r}\left(\frac{\partial\Theta}{\partial\theta}\right)\left(\frac{\partial R}{\partial r}\right)\frac{\partial^2 r}{\partial\Theta\partial R} + \frac{(2\beta+1)}{r}\frac{\partial^2\theta}{\partial\Theta^2}\left(\frac{\partial\Theta}{\partial\theta}\right)^2 \right) \right)$$
$$+ \mu\left(J^{-2\beta}\left(\frac{2\beta\cot\theta}{r} - \frac{2\beta\cot\Theta}{r}\frac{\partial\Theta}{\partial\theta} \right) + \frac{2}{R^2}\left(\frac{\partial\theta}{\partial\Theta}\right)\frac{\partial r}{\partial\Theta} + \frac{r}{R^2}\frac{\partial^2\theta}{\partial\Theta^2} \right), \tag{54}$$

also

$$\frac{1}{r}\frac{\partial S_2^1}{\partial R} = \mu J^{-2\beta}\left(-\frac{4\beta}{r^2}\left(\frac{\partial\Theta}{\partial\theta}\right)\left(\frac{\partial r}{\partial\Theta}\right) - \frac{2\beta}{r}\left(\frac{\partial\Theta}{\partial\theta}\right)\left(\frac{\partial R}{\partial r}\right)^2\left(\frac{\partial r}{\partial\Theta}\right)\frac{\partial^2 r}{\partial R^2}\right)$$

$$+\mu J^{-2\beta}\left(\frac{4\beta}{rR}\left(\frac{\partial\Theta}{\partial\theta}\right)\left(\frac{\partial R}{\partial r}\right)\frac{\partial r}{\partial\Theta} + \frac{1}{r}\left(\frac{\partial\Theta}{\partial\theta}\right)\frac{\partial^2 r}{\partial R\partial\Theta}\left(\frac{\partial R}{\partial r}\right) - \frac{1}{r}\left(\frac{\partial\Theta}{\partial\theta}\right)\left(\frac{\partial R}{\partial r}\right)^2\frac{\partial r}{\partial\Theta}\left(\frac{\partial^2 r}{\partial R^2}\right)\right),$$

$$(55)$$

similarly

$$-\frac{S_2^2}{r^2}\frac{\partial r}{\partial\Theta} = \mu\left(\frac{J^{-2\beta}}{r^2}\left(\frac{\partial\Theta}{\partial\theta}\right)\frac{\partial r}{\partial\Theta} - \frac{1}{R^2}\frac{\partial\theta}{\partial\Theta}\left(\frac{\partial r}{\partial\Theta}\right)\right), \tag{56}$$

and

$$-\frac{S_2^1}{r^2}\left(\frac{\partial r}{\partial R}\right) = -\frac{\mu J^{-2\beta}}{r^2}\left(\frac{\partial r}{\partial\Theta}\right)\frac{\partial\Theta}{\partial\theta}, \tag{57}$$

where

$$\frac{2S_2^1}{Rr} = \frac{2\mu J^{-2\beta}}{Rr}\left(\frac{\partial\Theta}{\partial\theta}\right)\frac{\partial R}{\partial r}\left(\frac{\partial r}{\partial\Theta}\right), \tag{58}$$

and

$$\frac{S_2^2\cot\Theta}{r} = \mu\left(-\frac{J^{-2\beta}}{r}\cot\Theta\frac{\partial\Theta}{\partial\theta} + \frac{r}{R^2}\cot\Theta\frac{\partial\theta}{\partial\Theta}\right). \tag{59}$$

Other angular terms lead to

$$\frac{-S_3^3\cot\theta}{r} = \mu\left(\frac{J^{-2\beta}\cot\theta}{r} - \frac{r\sin\theta\cos\theta}{R^2\sin^2\Theta}\right), \tag{60}$$

and

$$S_1^2\left(\frac{\partial\theta}{\partial\Theta}\right) = \frac{\mu}{R^2}\left(\frac{\partial r}{\partial\Theta}\right)\frac{\partial\theta}{\partial\Theta}. \tag{61}$$

Combining equations (53) to (61) and substituting into equation (39) gives

$$
J^{-2\beta}\left(\frac{(2\beta+1)}{r}\frac{\partial\Theta}{\partial\theta}\left(\frac{\partial R}{\partial r}\right)\frac{\partial^2 r}{\partial\Theta\partial R}+\frac{(2\beta+1)}{r}\left(\frac{\partial\Theta}{\partial\theta}\right)^2\frac{\partial^2\theta}{\partial\Theta^2}+\frac{(2\beta+1)\cot\theta}{r}\right)
$$

$$
+J^{-2\beta}\left(-\frac{(2\beta+1)\cot\Theta}{r}\left(\frac{\partial\Theta}{\partial\theta}\right)-\frac{(2\beta+1)}{r}\left(\frac{\partial\Theta}{\partial\theta}\right)\left(\frac{\partial R}{\partial r}\right)^2\left(\frac{\partial r}{\partial\Theta}\right)\frac{\partial^2 r}{\partial R^2}\right)
$$

$$
+J^{-2\beta}\left(\frac{2(2\beta+1)}{rR}\left(\frac{\partial\Theta}{\partial\theta}\right)\frac{\partial R}{\partial r}\left(\frac{\partial r}{\partial\Theta}\right)\right)+\frac{2}{R^2}\left(\frac{\partial\theta}{\partial\Theta}\right)\frac{\partial r}{\partial\Theta}+\frac{r}{R^2}\frac{\partial^2\theta}{\partial\Theta^2}
$$

$$
+\frac{r}{R^2}\left(\frac{\partial\theta}{\partial\Theta}\right)\cot\Theta-\frac{r\sin\theta\cos\theta}{R^2\sin^2\Theta}=0. \quad (62)
$$

Both the radial and angular equations given by (52) and (62) can be rearranged and expressed in terms of their respective second partial derivatives with respect to Θ resulting in

$$
\frac{\partial^2 r}{\partial\Theta^2}=-R^2\frac{\partial^2 r}{\partial R^2}\left(1+(2\beta+1)J^{-2\beta}\left(\frac{\partial R}{\partial r}\right)^2\right)
$$

$$
+J^{-2\beta}\left(-\frac{4\beta R^2}{r}+4\beta R\left(\frac{\partial R}{\partial r}\right)+2R\left(\frac{\partial R}{\partial r}\right)-\frac{2R^2}{r}\right)
$$

$$
-2R\left(\frac{\partial r}{\partial R}\right)+r\left(\frac{\partial\theta}{\partial\Theta}\right)^2+\frac{r\sin^2\theta}{\sin^2\Theta}-\cot\Theta\frac{\partial r}{\partial\Theta}, \quad (63)
$$

and

$$
\left(\frac{(2\beta+1)}{r}J^{-2\beta}\left(\frac{\partial\Theta}{\partial\theta}\right)^2+\frac{r}{R^2}\right)\frac{\partial^2\theta}{\partial\Theta^2}
$$

$$
=J^{-2\beta}\left(-\frac{(2\beta+1)}{r}\left(\frac{\partial\Theta}{\partial\theta}\right)\left(\frac{\partial R}{\partial r}\right)\frac{\partial^2 r}{\partial\Theta\partial R}-\frac{(2\beta+1)\cot\theta}{r}+\frac{(2\beta+1)\cot\Theta}{r}\left(\frac{\partial\Theta}{\partial\theta}\right)\right)
$$

$$
+J^{-2\beta}\left(\frac{(2\beta+1)}{r}\left(\frac{\partial\Theta}{\partial\theta}\right)\left(\frac{\partial R}{\partial r}\right)^2\left(\frac{\partial r}{\partial\Theta}\right)\frac{\partial^2 r}{\partial R^2}-\frac{2(2\beta+1)}{rR}\left(\frac{\partial\Theta}{\partial\theta}\right)\left(\frac{\partial R}{\partial r}\right)\frac{\partial r}{\partial\Theta}\right)
$$

$$
-\frac{2}{R^2}\left(\frac{\partial\theta}{\partial\Theta}\right)\frac{\partial r}{\partial\Theta}-\frac{r\cot\Theta}{R^2}\left(\frac{\partial\theta}{\partial\Theta}\right)+\frac{r\sin\theta\cos\theta}{R^2\sin^2\Theta}. \quad (64)
$$

7 Nondimensionalisation

In this section, the radial and angular equations are nondimensionalised. The radial and angular equations are nondimensionalised using $y = r/R_I$ and $Y = R/R_I$ where $Y_I = 1$ and $Y_O = R_O/R_I$. The equation for the quasistatic radial momentum represented by equation (63) gives

$$
\frac{\partial^2 y}{\partial \Theta^2} = -Y^2 \frac{\partial^2 y}{\partial Y^2} \left(1 + (2\beta + 1) J^{-2\beta} \left(\frac{\partial Y}{\partial y} \right)^2 \right)
$$
$$
+ J^{-2\beta} \left(-\frac{4\beta Y^2}{y} + 4\beta Y \left(\frac{\partial Y}{\partial y} \right) + 2Y \left(\frac{\partial Y}{\partial y} \right) - \frac{2Y^2}{y} \right)
$$
$$
- 2Y \left(\frac{\partial y}{\partial Y} \right) + y \left(\frac{\partial \theta}{\partial \Theta} \right)^2 + \frac{y \sin^2 \theta}{\sin^2 \Theta} - \cot \Theta \frac{\partial y}{\partial \Theta}, \quad (65)
$$

where the Jacobian given by equation (14) has a nonlinearised form given by

$$
J = \frac{y^2}{Y^2} \left(\frac{\partial y}{\partial Y} \right) \left(\frac{\partial \theta}{\partial \Theta} \right) \frac{\sin \theta}{\sin \Theta}. \quad (66)
$$

The quasistatic polar momentum equation represented by equation (64) reduces to

$$
\left(\frac{(2\beta + 1)}{y} J^{-2\beta} \left(\frac{\partial \Theta}{\partial \theta} \right)^2 + \frac{y}{Y^2} \right) \frac{\partial^2 \theta}{\partial \Theta^2}
$$
$$
= J^{-2\beta} \left(-\frac{(2\beta + 1)}{y} \left(\frac{\partial \Theta}{\partial \theta} \right) \left(\frac{\partial Y}{\partial y} \right) \frac{\partial^2 y}{\partial \Theta \partial Y} - \frac{(2\beta + 1) \cot \theta}{y} + \frac{(2\beta + 1) \cot \Theta}{y} \left(\frac{\partial \Theta}{\partial \theta} \right) \right)
$$
$$
+ J^{-2\beta} \left(\frac{(2\beta + 1)}{y} \left(\frac{\partial \Theta}{\partial \theta} \right) \left(\frac{\partial Y}{\partial y} \right)^2 \left(\frac{\partial y}{\partial \Theta} \right) \frac{\partial^2 y}{\partial Y^2} - \frac{2(2\beta + 1)}{yY} \left(\frac{\partial \Theta}{\partial \theta} \right) \left(\frac{\partial Y}{\partial y} \right) \frac{\partial y}{\partial \Theta} \right)
$$
$$
- \frac{2}{Y^2} \left(\frac{\partial \theta}{\partial \Theta} \right) \frac{\partial y}{\partial \Theta} - \frac{y \cot \Theta}{Y^2} \left(\frac{\partial \theta}{\partial \Theta} \right) + \frac{y \sin \theta \cos \theta}{Y^2 \sin^2 \Theta}, \quad (67)
$$

and the Cauchy stresses given by equations (41), (42), (43) and (44) lead to

$$\hat{\tau}_{yy} = \frac{\tau_{yy}}{\mu} = \frac{1}{J}\left(-J^{-2\beta} + \left(\frac{\partial y}{\partial Y}\right)^2 + \frac{1}{Y^2}\left(\frac{\partial y}{\partial \Theta}\right)^2\right), \tag{68}$$

alongside

$$\hat{\tau}_{\theta\theta} = \frac{\tau_{\theta\theta}}{\mu} = \frac{1}{J}\left(-J^{-2\beta} + \left(\frac{y}{Y}\right)^2\left(\frac{\partial \theta}{\partial \Theta}\right)^2\right), \tag{69}$$

and

$$\hat{\tau}_{\phi\phi} = \frac{\tau_{\phi\phi}}{\mu} = \frac{1}{J}\left(-J^{-2\beta} + \left(\frac{y\sin\theta}{Y\sin\Theta}\right)^2\right), \tag{70}$$

with the off diagonal stress term given by

$$\hat{\tau}_{y\theta} = \frac{\tau_{y\theta}}{\mu} = \frac{y}{JY^2}\left(\frac{\partial \theta}{\partial \Theta}\right)\frac{\partial y}{\partial \Theta}. \tag{71}$$

8   Linearisation of the radial and angular equations

In this section the radial and angular equations are linearised. Linearisation can be applied to both the radial and angular equations provided that the applied stress p is small compared to μ. Now consider the linearisation of the nondimensionalised radial equation (63) where

$$y(Y, \Theta) = Y + \epsilon f(Y, \Theta), \tag{72}$$

and

$$\theta(\Theta) = \Theta + \epsilon g(\Theta), \tag{73}$$

where $\epsilon = \hat{p} = p/\mu$ and is small in magnitude (0.0002μ), $\epsilon f(Y, \Theta)$ represents a small radial perturbation and $\epsilon g(\Theta)$ denotes a small angular perturbation. Consider the following expressions for the partial derivatives of the nondimensionalised equations (72) and (73),

$$\frac{\partial y}{\partial Y} = 1 + \epsilon \frac{\partial f}{\partial Y},$$
$$\frac{\partial \theta}{\partial \Theta} = 1 + \epsilon \frac{dg}{d\Theta}.$$

Linearising the Jacobian, J, given by equation (14) requires the simplification $\sin \theta = \sin \Theta + \epsilon g \cos \Theta$ resulting in

$$\frac{\sin \theta}{\sin \Theta} = 1 + \epsilon g \cot \Theta,$$

and substituting into equation (14) gives

$$J = \frac{(Y + \epsilon f)^2}{Y^2} \left(1 + \epsilon \frac{\partial f}{\partial Y}\right) \left(1 + \epsilon \frac{dg}{d\Theta}\right) (1 + \epsilon g \cot \Theta),$$
$$\approx 1 + \frac{2\epsilon f}{Y} + \epsilon \frac{\partial f}{\partial Y} + \epsilon \frac{dg}{d\Theta} + \epsilon g \cot \Theta, \tag{74}$$

and hence

$$J^{-2\beta} \approx 1 - 2\beta\epsilon \left(\frac{2f}{Y} + \frac{\partial f}{\partial Y} + \frac{dg}{d\Theta} + g \cot \Theta\right). \tag{75}$$

Terms in equation (63) become

$$1 + (2\beta + 1) J^{-2\beta} \left(\frac{\partial Y}{\partial y}\right)^2 \approx 1 + (2\beta + 1) \left(1 - 2\beta\epsilon \left(\frac{2f}{Y} + \frac{\partial f}{\partial Y} + \frac{dg}{d\Theta} + g \cot \Theta\right)\right) \left(1 - 2\epsilon \frac{\partial f}{\partial Y}\right),$$
$$\approx 2(\beta + 1) - 2(2\beta + 1)\epsilon \left(\frac{2\beta f}{Y} + (\beta + 1)\frac{\partial f}{\partial Y} + \beta \frac{dg}{d\Theta} + \beta g \cot \Theta\right), \tag{76}$$

and

$$-Y^2 \frac{\partial^2 y}{\partial Y^2} \left(1 + (2\beta + 1)J^{-2\beta} \left(\frac{\partial Y}{\partial y}\right)^2\right) \approx -2Y^2(1 + \beta)\epsilon \frac{\partial^2 f}{\partial Y^2}. \qquad (77)$$

The following term in equation (63)

$$J^{-2\beta} \left(-\frac{4\beta Y^2}{y} + 4\beta Y \left(\frac{\partial Y}{\partial y}\right) + 2Y \left(\frac{\partial Y}{\partial y}\right) - \frac{2Y^2}{y}\right), \qquad (78)$$

can use the following linearised terms

$$\frac{-4\beta Y^2}{y} = \frac{-4\beta Y^2}{(Y + \epsilon f)} \approx -4\beta Y + 4\epsilon\beta f, \qquad (79)$$

and

$$4\beta Y \left(\frac{\partial Y}{\partial y}\right) = \frac{4\beta Y}{\left(1 + \epsilon \frac{\partial f}{\partial Y}\right)} \approx 4\beta Y - 4\beta\epsilon Y \left(\frac{\partial f}{\partial Y}\right), \qquad (80)$$

also

$$2Y \left(\frac{\partial Y}{\partial y}\right) = \frac{2Y}{\left(1 + \epsilon \frac{\partial f}{\partial Y}\right)} \approx 2Y - 2\epsilon Y \frac{\partial f}{\partial Y}, \qquad (81)$$

similarly

$$\frac{-2Y^2}{y} = \frac{-2Y^2}{(Y + \epsilon f)} \approx -2Y + 2\epsilon f, \qquad (82)$$

to give

$$J^{-2\beta} \left(-\frac{4\beta Y^2}{y} + 4\beta Y \left(\frac{\partial Y}{\partial y}\right) + 2Y \left(\frac{\partial Y}{\partial y}\right) - \frac{2Y^2}{y}\right) \approx 2(2\beta + 1)\epsilon \left(f - Y \left(\frac{\partial f}{\partial Y}\right)\right).$$
$$(83)$$

Linearising the following terms from equation (63) results in

$$- 2Y \left(\frac{\partial y}{\partial Y}\right) \approx -2Y - 2\epsilon Y \left(\frac{\partial f}{\partial Y}\right), \qquad (84)$$

also

$$y \left(\frac{\partial \theta}{\partial \Theta} \right)^2 = (Y + \epsilon f) \left(1 + \epsilon \frac{dg}{d\Theta} \right)^2 \approx Y + 2\epsilon Y \left(\frac{dg}{d\Theta} \right) + \epsilon f, \qquad (85)$$

similarly

$$\frac{y \sin^2 \theta}{\sin^2 \Theta} = (Y + \epsilon f) \left(1 + \epsilon g \cot \Theta \right)^2 \approx Y + 2\epsilon Y g \cot \Theta + \epsilon f, \qquad (86)$$

and

$$- \cot \Theta \left(\frac{\partial y}{\partial \Theta} \right) \approx - \cot \Theta \left(\epsilon \frac{\partial f}{\partial \Theta} \right). \qquad (87)$$

Collecting the expressions (77) and (83) to (87) and substituting into equation (63) reduces equation (63) on rearrangement, to

$$- (4\beta + 4) Y \frac{\partial f}{\partial Y} + (4\beta + 4) f + 2Y g \cot \Theta + 2Y \frac{dg}{d\Theta}$$
$$- \cot \Theta \frac{\partial f}{\partial \Theta} - \frac{\partial^2 f}{\partial \Theta^2} - 2Y^2 (\beta + 1) \frac{\partial^2 f}{\partial Y^2} = 0, \quad (88)$$

which can be further rearranged and results in

$$(4\beta + 4) f - (4\beta + 4) Y \frac{\partial f}{\partial Y} - \cot \Theta \frac{\partial f}{\partial \Theta} - \frac{\partial^2 f}{\partial \Theta^2} - 2Y^2 (\beta + 1) \frac{\partial^2 f}{\partial Y^2}$$
$$= -2Y g \cot \Theta - 2Y \frac{dg}{d\Theta}. \quad (89)$$

Linearising the angular equation given by equation (64) requires the following expressions

$$J^{-2\beta} \left(\frac{-(2\beta + 1)}{y} \right) \left(\frac{\partial \Theta}{\partial \theta} \right) \left(\frac{\partial Y}{\partial y} \right) \frac{\partial^2 y}{\partial \Theta \partial Y} \approx \frac{-(2\beta + 1)}{Y} \epsilon \frac{\partial^2 f}{\partial Y \partial \Theta}, \qquad (90)$$

simplifying $\cot \theta$ yields

$$\cot \theta = \frac{\cos(\Theta + \epsilon g)}{\sin(\Theta + \epsilon g)},$$

$$\approx \cot \Theta - \epsilon g \csc^2 \Theta, \tag{91}$$

leading to

$$\frac{-(2\beta + 1)\cot \theta}{y} = \frac{-(2\beta + 1)(\cot \Theta - \epsilon g \csc^2 \Theta)}{(Y + \epsilon f)},$$

$$\approx \frac{-(2\beta + 1)}{Y}\left(\cot \Theta - \epsilon g \csc^2 \Theta - \epsilon \frac{f}{Y}\cot \Theta\right), \tag{92}$$

which results in

$$-J^{-2\beta}\frac{(2\beta + 1)\cot \theta}{y} \approx \frac{-(2\beta + 1)\cot \Theta}{Y} + \frac{(2\beta + 1)(4\beta + 1)\epsilon f \cot \Theta}{Y^2}$$

$$+ \frac{(2\beta + 1)\epsilon g}{Y}(\beta + 1 + \beta \cos 2\Theta)\csc^2 \Theta$$

$$+ \frac{2\beta(2\beta + 1)}{R}\epsilon \left(\cot \Theta \frac{dg}{d\Theta} + \cot \Theta \frac{\partial f}{\partial Y}\right). \tag{93}$$

Consider

$$\frac{(2\beta + 1)\cot \Theta}{y}\left(\frac{\partial \Theta}{\partial \theta}\right) \approx \frac{(2\beta + 1)\cot \Theta}{Y}\left(1 - \epsilon \frac{f}{Y} - \epsilon \frac{dg}{d\Theta}\right), \tag{94}$$

and combining expression (94) with $J^{-2\beta}$ gives

$$J^{-2\beta}\frac{(2\beta + 1)\cot \Theta}{y}\left(\frac{\partial \Theta}{\partial \theta}\right) \approx \frac{(2\beta + 1)\cot \Theta}{Y}$$

$$- \epsilon \frac{(2\beta + 1)\cot \Theta}{Y^2}\left((1 + 4\beta)f + Y\left((2\beta + 1)\frac{dg}{d\Theta} + 2\beta g \cot \Theta + 2\beta \frac{\partial f}{\partial Y}\right)\right). \tag{95}$$

The following expression leads to

$$\frac{(2\beta + 1)}{y} \left(\frac{\partial \Theta}{\partial \theta}\right) \left(\frac{\partial Y}{\partial y}\right)^2 \left(\frac{\partial y}{\partial \Theta}\right) \frac{\partial^2 y}{\partial Y^2},$$

$$\approx \frac{(2\beta + 1)}{(Y + \epsilon f)} \left(1 - \epsilon \frac{dg}{d\Theta}\right) \left(1 - 2\epsilon \frac{\partial f}{\partial Y}\right) \left(\epsilon \frac{\partial f}{\partial \Theta}\right) \epsilon \frac{\partial^2 f}{\partial Y^2} = 0. \tag{96}$$

Now considering

$$\frac{-2(2\beta + 1)}{yY} \left(\frac{\partial \Theta}{\partial \theta}\right) \left(\frac{\partial Y}{\partial y}\right) \frac{\partial y}{\partial \Theta} \approx \frac{-2(2\beta + 1)}{Y^2} \epsilon \left(\frac{\partial f}{\partial \Theta}\right), \tag{97}$$

which on combining with $J^{-2\beta}$ results in

$$J^{-2\beta} \left(\frac{-2(2\beta + 1)}{yY} \left(\frac{\partial \Theta}{\partial \theta}\right) \left(\frac{\partial Y}{\partial y}\right) \frac{\partial y}{\partial \Theta}\right) \approx \frac{-2(2\beta + 1)}{Y^2} \epsilon \left(\frac{\partial f}{\partial \Theta}\right). \tag{98}$$

Other terms are

$$\frac{-2}{Y^2} \left(\frac{\partial \theta}{\partial \Theta}\right) \left(\frac{\partial y}{\partial \Theta}\right) \approx \frac{-2\epsilon}{Y^2} \left(\frac{\partial f}{\partial \Theta}\right), \tag{99}$$

and

$$\frac{-y \cot \Theta}{Y^2} \left(\frac{\partial \theta}{\partial \Theta}\right) \approx \frac{-\cot \Theta}{Y} - \frac{\epsilon \cot \Theta}{Y} \left(\frac{dg}{d\Theta}\right) - \frac{\epsilon f \cot \Theta}{Y^2}. \tag{100}$$

Now since $\sin \theta \approx \sin \Theta + \epsilon g \cos \Theta$ similarly, $\cos \theta \approx \cos \Theta - \epsilon g \sin \Theta$, resulting in

$$\sin \theta \cos \theta \approx \sin \Theta \cos \Theta + \epsilon g \left(1 - 2 \sin^2 \Theta\right), \tag{101}$$

then

$$\frac{y \sin \theta \cos \theta}{Y^2 \sin^2 \Theta} \approx \frac{1}{Y} \left(\left(1 + \frac{\epsilon f}{Y}\right) \cot \Theta + \epsilon g(\cot^2 \Theta - 1)\right), \tag{102}$$

also

$$\frac{(2\beta + 1)}{y}J^{-2\beta}\left(\frac{\partial\Theta}{\partial\theta}\right)^2 + \frac{y}{Y^2},$$
$$\approx \frac{(2\beta + 1)}{Y}\left(1 - \frac{\epsilon f}{Y} - 2\epsilon\frac{dg}{d\Theta} - 2\beta\epsilon\left(\frac{2f}{Y} + \frac{\partial f}{\partial Y} + \frac{dg}{d\Theta} + g\cot\Theta\right)\right) + \frac{1}{Y}\left(1 + \frac{\epsilon f}{Y}\right),$$

(103)

which on combining expression (103) with $\partial^2\theta/\partial\Theta^2$ leads to

$$\frac{(2\beta + 1)\epsilon}{Y}\left(\frac{d^2g}{d\Theta^2}\right) + \frac{\epsilon}{Y}\left(\frac{d^2g}{d\Theta^2}\right) \approx \frac{2(\beta + 1)\epsilon}{Y}\left(\frac{d^2g}{d\Theta^2}\right).$$

(104)

Combining and substituting equations (90), (92), (93), (95) to (100) and (102) and (104) into the angular equation (64) results in

$$-Y\left(1 + 2\beta + \cos^2\Theta\right)g\csc^2\Theta + 2Y(1 + \beta)\cot\Theta\left(\frac{dg}{d\Theta}\right)$$
$$+ 2Y(1 + \beta)\frac{d^2g}{d\Theta^2} + 4(1 + \beta)\left(\frac{\partial f}{\partial\Theta}\right)$$
$$+ Y(1 + 2\beta)\frac{\partial^2 f}{\partial Y\partial\Theta} = 0. \quad (105)$$

9 Linearisation of the Cauchy stresses

In this next section we will linearise the Cauchy stresses. The Cauchy radial, polar and azimuthal stresses given by equations (68), (69) and (70) respectively are linearised using equations (72) and (73) which results in

$$\hat{\tau}_{yy} \approx \epsilon\left(\frac{4\beta f}{Y} + (2\beta + 2)\frac{\partial f}{\partial Y} + 2\beta\frac{dg}{d\Theta} + 2\beta g\cot\Theta\right),$$

(106)

alongside

$$\hat{\tau}_{\theta\theta} \approx \epsilon \left((4\beta + 2)\frac{f}{Y} + 2\beta \left(\frac{\partial f}{\partial Y} \right) + (2\beta + 2) \left(\frac{dg}{d\Theta} \right) + 2\beta g \cot \Theta \right), \qquad (107)$$

and

$$\hat{\tau}_{\phi\phi} \approx \epsilon \left((4\beta + 2)\frac{f}{Y} + 2\beta \left(\frac{\partial f}{\partial Y} \right) + 2\beta \left(\frac{dg}{d\Theta} \right) + (2\beta + 2)g \cot \Theta \right), \qquad (108)$$

respectively. Equations (106) and (107) will be used to evaluate the boundary conditions for both the deformation of the open shell (forward picture) and the collapse phase of the shell.

10 Boundary conditions for the deformation the shell - the forward picture

In this section we will discuss the boundary conditions for the forward picture. From the definition of the Jacobian, J, given by equation (14) we can observe that there is a coordinate singularity at the the north pole of the shelled microbubble. To overcome this coordinate singularity at $\Theta = 0$, the domain is partitioned into two regions. The first region restricts the polar angle Θ to a very small angular region. In this region the angular dependency is approximated by $\theta(\Theta) = \Theta$ which imples that the shell's behaviour is purely radial and compressive. This region is defined by $0 \leq \Theta \leq \Theta_s$ where Θ_s represents the boundary of the purely radial and compressive region at the north pole. This imples that the region which is purely radially dependent has an angular perturbation such that $g(\Theta) = 0$ resulting in $\theta(\Theta) = \Theta$. The second region is much larger and effectively covers the remaining sphere. This second region is compressible and exhibits both an angular and radial

30

dependency such that $r = r(R, \Theta)$ and $\theta = \theta(\Theta)$ and is restricted to $\Theta_s < \Theta \leq \Theta_{op}$ where Θ_{op} is the opening angle. A matching boundary condition is applied at Θ_s to both the radial and angular equations. Note that the opening polar angle is defined as the supplement of an angle, Θ_{op}, such that the opening angle is given by $\pi - \Theta_{op}$ where Θ_{op} is large and its supplement (the opening angle) is small. The boundary conditions at the nondimensionalised inner and outer radii of the shell (which are represented by Y_I and Y_O respectively) are obtained using the nondimensionalised Cauchy radial stresses where $\hat{\tau}_{yy}(Y_I) = 0$ and $\hat{\tau}_{yy}(Y_O) = 0$. Using equation (106) and setting $\hat{\tau}_{yy} = 0$ at both the nondimensionalised inner and outer radii $Y_{I/O}$ leads to

$$\frac{4\beta f(Y_{I/O}, \Theta)}{Y_{I/O}} + (2\beta + 2)\frac{\partial f(Y_{I/O}, \Theta)}{\partial Y} + 2\beta\frac{dg}{d\Theta} + 2\beta g \cot \Theta = 0. \tag{109}$$

The polar angular boundary condition at Θ_s is given by

$$g(\Theta_s) = 0, \tag{110}$$

resulting in $\theta(\Theta) = \Theta$. At the opening angle Θ_{op} the polar hoop stress represented by equation (107) is subjected to a nondimensionalised stress $\hat{p}$ where $\hat{p} = p/\mu$ and $\epsilon = \hat{p}$. This small stress applied to the surface of the shell deforms the shell. The boundary condition is evaluated using

$$\hat{\tau}_{\theta\theta}(\Theta_{op}) = \hat{p} = \epsilon. \tag{111}$$

This simplifies using equation (107) to give

$$\frac{(4\beta + 2)f}{Y} + 2\beta\frac{\partial f}{\partial Y} + (2\beta + 2)\frac{dg}{d\Theta} + 2\beta g \cot \Theta_{op} = 1. \tag{112}$$

at Θ_{op}.

11 Solving the angular and radial equation for the forward picture - deformation of the shell

In this next section we will solve the radial and angular equations for the forward picture. To solve the radial and angular equations represented by equations (89) and (105) we shall consider the case when $\nu \to 1/2$. We will assume that the angular equation is independent of Y thus for large β equation (105) reduces to

$$g'' + \cot \Theta g' - g(\csc \Theta)^2 = 0, \tag{113}$$

where

$$\frac{d}{d\Theta} \left(g \cot \Theta + g' \right) = 0,$$

$$\text{thus } g' + g \cot \Theta = \text{a constant.} \tag{114}$$

To determine the constant in equation (114) we can apply the boundary condition at the opening angle which is represented by equation (112) by assuming that $\hat{\tau}_{\theta\theta}(\Theta_{op})$ is independent of Y (see Figure 3). This assumption allows us to gain analytical insight into the problem. The boundary condition at Θ_{op} for large β leads to

$$\frac{dg}{d\Theta} + g \cot \Theta_{op} = \frac{1}{2\beta}. \tag{115}$$

Equation (115) places a value on the constant in equation (114) where the constant $= 1/(2\beta)$. This leads to

$$g' + g \cot \Theta = \frac{1}{2\beta}, \tag{116}$$

which results in

$$\frac{d}{d\Theta}\left(g\sin\Theta\right) = \frac{\sin\Theta}{2\beta},$$

$$\text{and } g(\Theta) = -\frac{\cos\Theta}{2\beta} + k\csc\Theta. \tag{117}$$

Applying the angular boundary condition at Θ_s where $g(\Theta_s) = 0$ gives $k = \cos\Theta_s/(2\beta)$ resulting in

$$g(\Theta) = -\frac{\cot\Theta}{2\beta} + \frac{\cos\Theta_s\csc\Theta}{2\beta}. \tag{118}$$

For large β the radial equation given by equation (89) reduces to

$$4\beta f - 4\beta Y\frac{\partial f}{\partial Y} - \cot\Theta\frac{\partial f}{\partial\Theta} - \frac{\partial^2 f}{\partial\Theta^2} - 2Y^2\beta\frac{\partial^2 f}{\partial Y^2} = -2Yg\cot\Theta - 2Y\frac{dg}{d\Theta} = -\frac{2Y}{2\beta} \approx 0, \tag{119}$$

as $\beta \to \infty$. Considering

$$4\beta f - 4\beta Y\frac{\partial f}{\partial Y} - \cot\Theta\frac{\partial f}{\partial\Theta} - \frac{\partial^2 f}{\partial\Theta^2} - 2Y^2\beta\frac{\partial^2 f}{\partial Y^2} = 0, \tag{120}$$

and solving using separation of variables where $f(Y,\Theta) = a(Y)b(\Theta)$ leads to

$$4\beta - 4\beta Y\frac{a'}{a} - 2Y^2\beta\frac{a''}{a} = \cot\Theta\frac{b'}{b} + \frac{b''}{b} = K, \tag{121}$$

which can be rewritten as

$$b'' + b'\cot\Theta - Kb = 0, \tag{122}$$

$$-2Y^2\beta a'' - 4\beta Y a' + (4\beta - K)\,a = 0. \tag{123}$$

33

Equation (123) is solved by setting $a(Y) = Y^s$ which leads to

$$s^2 + s + \frac{K - 4\beta}{2\beta} = 0, \tag{124}$$

which has solution(s)

$$s = \frac{-1 \pm \sqrt{1 - 4(K - 4\beta)/(2\beta)}}{2}, \tag{125}$$

where $a(Y) = c_i Y^s$ and c_i is determined by applying the boundary conditions for the radial equation at $Y_{I/O}$. Note that at $K = 9\beta/2$ equation (125) reduces to one solution only which is the condition for equal roots. Applying the radial boundary condition given by equation (112) due to $\hat{\tau}_{yy} = 0$ and using separation of variables leads to

$$4\beta \frac{ab}{Y} + (2\beta + 2) a'b + 2\beta \left(g' + g \cot \Theta \right) = 0, \tag{126}$$

and since $g' + g \cot \Theta \approx 0$ for $\beta \to \infty$ equation (126) simplifies to

$$b \left(4\beta \frac{a}{Y} + 2\beta a' \right) = 0,$$
$$\text{thus } \frac{2a}{Y_{I/O}} + a'(Y_{I/O}) = 0, \tag{127}$$

at $Y_{I/O}$. For $b(\Theta)$ given by equation (122) we assume that at Θ_s any change in the radial positions of the particles in the shell at that position depends only on Y thus $f(Y, \Theta_s) = f(Y)$ with $a(Y)b(\Theta_s) = a(Y)$ therefore $b(\Theta_s) = 1$. The angular term $b(\Theta)$ represented by equation (122) is a Legendre function with boundary conditions $b(\Theta_s) = 1$ and $b'(\Theta_s) = 0$ at the matching boundary Θ_s. The general solution for $a(Y)$ is represented by $a(Y) = c_i Y^s$ where s is given by equation (125). This is solved by applying the boundary conditions at $Y_{I/O}$ given by equation (127) to $a(Y) = c_i Y^s$ which results in a 2×2 matrix, $M(K)$, whose determinant is plotted

versus K for a given value of β. Using a range of values for K results in a plot with two unique roots that occur at $K = 0$ and $K = 9\beta/2$. Figure 2 illustrates how the determinant of $a(Y) = c_i Y^s$ subjected to equation (127) varies with K where s is given by equation (125).
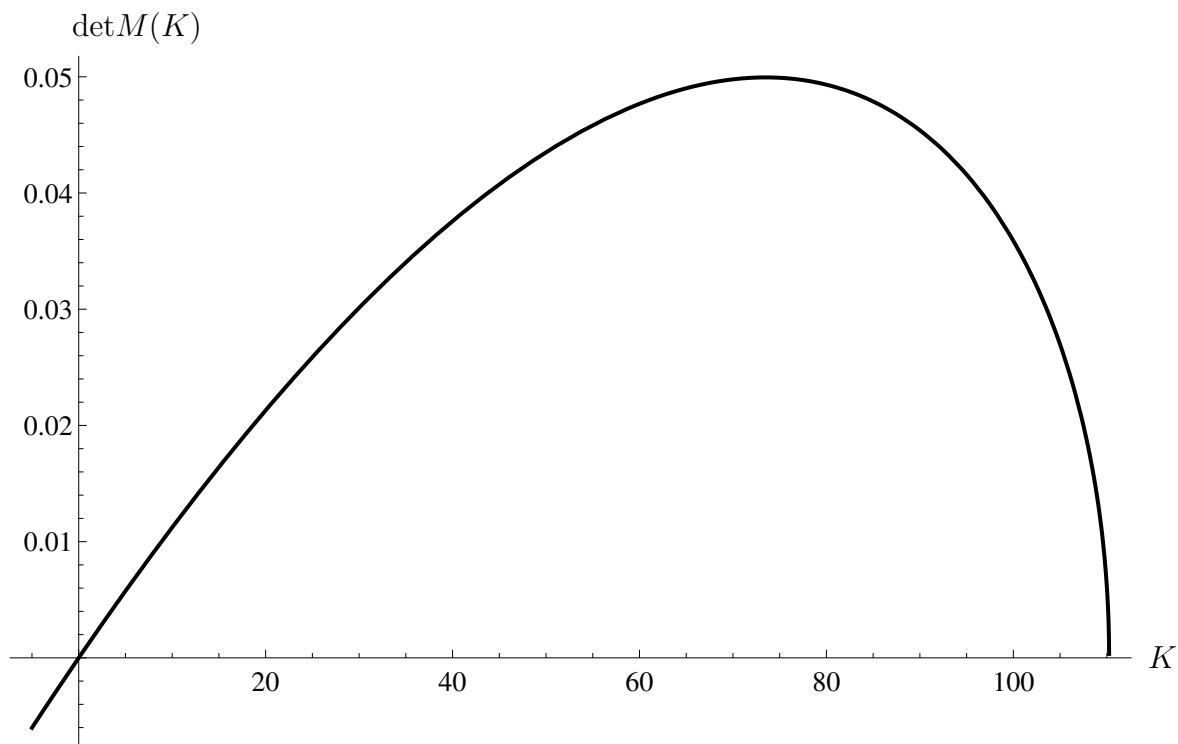

Figure 2: This is calculated using $a(Y) = c_i Y^s$ alonside equations (125) and (127).

For Figure 2 when $K = 0$ the solution is $a(Y) = c_1 Y + c_2/Y^2$ which has two linearly independent eigenvectors that lead to a trivial solution where $c_1 = c_2 = 0$. The nontrivial solution occurs when $K = 9\beta/2$ and has a solution represented by

$$a(Y) = c_1 Y^{-1/2} + c_2 Y^{-1/2} \log Y. \tag{128}$$

Applying the radial boundary conditions given by equation (127) to equation (128)

35

leads to $c_1 = -c_2/3$ resulting in

$$a(Y) = c_2 \left(-\frac{1}{3} Y^{-1/2} + Y^{-1/2} \log Y \right). \tag{129}$$

The angular expression $b(\Theta)$ which is given by equation (122) is solved for the boundary conditions $b(\Theta_s = 1$ and $b'(\Theta_s) = 0$. This can be solved numerically and is a Legendre function of the first and second kinds. To determine c_2 we apply the conservation of mass. The conservation of mass demands that

$$m_{ref} = m_{current}, \tag{130}$$

where $\rho_{ref} = \rho_{current} J$ and J is the Jacobian is given by equation (74). This leads to

$$V_{ref} = \int \frac{dV_{current}}{J}, \tag{131}$$

which is solved numerically to give a value for c_2 which is dependent on the opening angle Θ_{op}, the matching boundary condition Θ_s and the applied hoop (polar) stress $\hat{p}$ where $\hat{p} = p/\mu = \epsilon$.

12 Determining the collapse phase of the shell for the radial component of the momentum

This section will focus on the collapse phase of the shell. To collapse the shell we have to consider both the radial and angular components of the linear momentum where the radial component of the linear momentum is denoted by

$$\rho_o \frac{Dv}{Dt} = \nabla_R \cdot S, \tag{132}$$

and ρ_o is the density in the reference configuration, D/Dt is the material derivative and S is the first Piola Kirchoff stress tensor. Applying equation (132) to the radial component of the momentum gives

$$\left(\rho_o \frac{Dv_r}{Dt}\right) e_r = \nabla_R \cdot S, \tag{133}$$

where $v_r = \partial r/\partial t$, $v_\theta = r\partial\theta/\partial t$, $v_\phi = 0$ and the material derivative ([16], p354-p355) is written as

$$\frac{Dv_r}{Dt} = \frac{\partial v_r}{\partial t} + v_r \frac{\partial v_r}{\partial r_i} + \frac{v_\theta}{r}\frac{\partial v_r}{\partial \theta_i} - \frac{v_\theta^2}{r}. \tag{134}$$

To nondimensionalise the material derivative represented by equation (158) we set $t = \gamma\hat{t}$ which results in

$$\frac{Dv_r}{Dt} = \frac{R_I}{\gamma^2}\left(\frac{\partial^2 y}{\partial \hat{t}^2} + \frac{\partial y}{\partial \hat{t}}\frac{\partial}{\partial y_i}\left(\frac{\partial y}{\partial \hat{t}}\right) + \frac{\partial \theta}{\partial \hat{t}}\frac{\partial}{\partial \theta_i}\left(\frac{\partial y}{\partial \hat{t}}\right) - y\left(\frac{\partial \theta}{\partial \hat{t}}\right)^2\right), \tag{135}$$

where the radial momentum component is given by

$$\frac{\rho_o R_I^2}{\mu_o \gamma^2}\left(\frac{\partial^2 y}{\partial \hat{t}^2} + \frac{\partial y}{\partial \hat{t}}\frac{\partial}{\partial y_i}\left(\frac{\partial y}{\partial \hat{t}}\right) + \frac{\partial \theta}{\partial \hat{t}}\frac{\partial}{\partial \theta_i}\left(\frac{\partial y}{\partial \hat{t}}\right) - y\left(\frac{\partial \theta}{\partial \hat{t}}\right)^2\right) e_r = \mu_r \nabla_Y \cdot \hat{S}, \tag{136}$$

and $\hat{S}$ is the nondimensionalised First Piola Kirchoff stress. Note that we have used a relative nondimensionalised shear modulus $\mu_r = \mu/\mu_o$ where $\mu_o = 20$MPa in order to determine how varying the shear modulus influences the collapse time of the shell whilst keeping γ fixed as μ is varied. This will result in a nondimensionalised time $\hat{t}$ which varies as μ changes whilst γ remains fixed. Equation (136) is nondimensionalised by setting $\rho_o R_I^2/(\mu_o\gamma^2) = 1$ which simplifies equation (136)

to

$$\left(\frac{\partial^2 y}{\partial \hat{t}^2} + \frac{\partial y}{\partial \hat{t}}\frac{\partial}{\partial y_i}\left(\frac{\partial y}{\partial \hat{t}}\right) + \frac{\partial \theta}{\partial \hat{t}}\frac{\partial}{\partial \theta_i}\left(\frac{\partial y}{\partial \hat{t}}\right) - y\left(\frac{\partial \theta}{\partial \hat{t}}\right)^2\right)e_r = \mu_r \nabla_Y \cdot \hat{S}. \qquad (137)$$

To solve equation (137) we linearise where

$$y = Y + \epsilon j(Y, \Theta, \hat{t}), \qquad (138)$$

and only the first term $\partial^2 y/\partial \hat{t}^2$ is non-zero since all the remaining terms on the left handside of equation (137) are second order. The right hand side of equation (137) represented by $\mu_r \nabla_Y \cdot \hat{S}$, is evaluated using the quasistatic solution for the First Piola Kirchoff equation represented by equation (120) but with a caveat. In equation (120) which denotes the deformation of the shell and is quasistatic, the stresses can exhibit both a compressive and a stretching behaviour whereas in the collapse phase the stresses are effectively all negative in nature and are thus compressive only. To collapse the shell the signs of the relative terms in equation (120) are changed to represent a compression only behaviour. Applying the linearisation represented by equation (138) to the compression modified equation initially denoted by equation (120) results in

$$\frac{\partial^2 j}{\partial \hat{t}^2} = \mu_r\left(-4\beta j + 4\beta Y\frac{\partial j}{\partial Y} - \cot\Theta\frac{\partial j}{\partial \Theta} - \frac{\partial^2 j}{\partial \Theta^2} - 2Y^2\beta\frac{\partial^2 j}{\partial Y^2}\right). \qquad (139)$$

Using separation of variables where $j(Y, \Theta, \hat{t}) = A(Y)B(\Theta)T(\hat{t})$ and substituting into equation (139) gives

$$\frac{\ddot{T}}{T} = \mu_r\left(-4\beta + 4\beta Y\left(\frac{A'}{A}\right) - \cot\Theta\left(\frac{B'}{B}\right) - \left(\frac{B''}{B}\right) - 2Y^2\beta\left(\frac{A''}{A}\right)\right) = \omega^2,$$
$$(140)$$

38

which can be rewritten as

$$\mu_r \left(-4\beta + 4\beta Y \left(\frac{A'}{A} \right) - 2Y^2 \beta \left(\frac{A''}{A} \right) \right) - \omega^2 = \mu_r \left(\left(\frac{B''}{B} \right) + \cot\Theta \left(\frac{B'}{B} \right) \right) = K\mu_r. \tag{141}$$

Equation (141) leads to two key equations

$$B'' + B' \cot\Theta - KB = 0, \tag{142}$$

$$\mu_r \left(-4\beta + 4\beta Y \left(\frac{A'}{A} \right) - 2Y^2 \beta \left(\frac{A''}{A} \right) - K \right) - \omega^2 = 0, \tag{143}$$

where $K = 9\beta/2$ which is obtained from the forward picture. To solve equations (142) and (143) we must consider the initial conditions for the collapse phase where

$$y = Y + \epsilon a(Y)b(\Theta) = Y + \epsilon A(Y)B(\Theta)T(0), \tag{144}$$

$$\frac{\partial j(Y, \Theta, 0)}{\partial \hat{t}} = 0, \tag{145}$$

which leads to

$$B(\Theta) = b(\Theta), \tag{146}$$

$$A(Y) = a(Y)/T(0). \tag{147}$$

Substituting equation (146) into equation (142) gives equation (122), $b'' + b' \cot\Theta - Kb = 0$, from the forward (quasistatic) picture. Using equation (146) to solve equation (143) results in

$$\mu_r \left(-4\beta + 4\beta Y \left(\frac{a'}{a} \right) - 2Y^2 \beta \left(\frac{a''}{a} \right) - K \right) - \omega^2 = 0. \tag{148}$$

From the forward picture expressed by equation (123)

$$- 2Y^2 \beta a'' = 4\beta Y a' - (4\beta - K)a, \tag{149}$$

which upon substituting into equation (148) leads to

$$\omega^2 = \mu_r \left(8\beta Y \left(\frac{a'}{a} \right) - 8\beta \right), \tag{150}$$

where $a(Y)$ is given by equation (129). Solving equation (129) results in a general solution for $a(Y)$ as a function of $\hat{p}$ where $\hat{p} = p/\mu = \epsilon$ which has the form

$$a(Y) = -\frac{\hat{p}}{2\sqrt{Y}} \left(-\frac{2c_2}{3} + c_2 \log Y \right), \tag{151}$$

where c_2 is evaluated numerically by applying the conservation of mass. Similarly

$$\frac{a'(Y)}{a(Y)} = \frac{8 - 3 \log Y}{2Y \left(3 \log Y - 2 \right)}, \tag{152}$$

and

$$\frac{Y a'(Y)}{a(Y)} = \frac{8 - 3 \log Y}{2 \left(3 \log Y - 2 \right)}, \tag{153}$$

where $\log Y$ can be expanded about $Y_I = 1$ via a Taylor expansion series resulting in

$$\frac{Y a'(Y)}{a(Y)} \approx -2 - \frac{9}{4} (Y - 1). \tag{154}$$

Substituting equation (154) into equation (150) for ω^2 leads to

$$\omega^2 = 8\beta\mu_r \left(-3 - \frac{9}{4} (Y - 1) \right), \tag{155}$$

40

where $Y_I \leq Y \leq Y_O$. Since $Y_I = 1$ and $Y_O = 1.02$ then the dependency of ω on Y is negligible.

13 Determining the collapse phase of the shell for the polar component of the momentum

THis section will discuss the polar component during the collapse phase of the shell. As well as there being a radial component of momentum there is also an polar component of linear momentum. This is given by

$$\left(\rho_o \frac{Dv_\theta}{Dt} \right) e_\theta = \frac{1}{R} \nabla_\Theta \cdot S, \tag{156}$$

where

$$v_\theta = r \frac{\partial \theta}{\partial t}. \tag{157}$$

The material derivative is given by ([16], p354-355)

$$\frac{Dv_\theta}{Dt} = \frac{\partial v_\theta}{\partial t} + v_r \frac{\partial v_\theta}{\partial r_i} + \frac{v_\theta}{r} \frac{\partial v_\theta}{\partial \theta_i} + \frac{v_r v_\theta}{r}. \tag{158}$$

and nondimensionalising where $y = r/R_I, Y = R/R_I$ and $t = \gamma \hat{t}$ leads to

$$\frac{Dv_\theta}{Dt} = \frac{R_I}{\gamma^2} \left(\frac{\partial}{\partial \hat{t}} \left(y \frac{\partial \theta}{\partial \hat{t}} \right) + \frac{\partial y}{\partial \hat{t}} \frac{\partial}{\partial y_i} \left(y \frac{\partial \theta}{\partial \hat{t}} \right) + \left(\frac{\partial \theta}{\partial \hat{t}} \right) \frac{\partial}{\partial \theta_i} \left(y \frac{\partial \theta}{\partial \hat{t}} \right) + \frac{\partial y}{\partial \hat{t}} \left(\frac{\partial \theta}{\partial \hat{t}} \right) \right). \tag{159}$$

Linearising equation (159) where $\epsilon = \hat{p}$ using

$$\theta(\Theta, \hat{t}) = \Theta + \epsilon h(\Theta, \hat{t}), \tag{160}$$

results in

$$\frac{Dv_\theta}{Dt} = \frac{R_I Y}{\gamma^2} \left(\epsilon \frac{\partial^2 h}{\partial \hat{t}^2} \right), \qquad (161)$$

since the second, third and fourth terms in equation (159) are higher order. The nondimensionalised right hand side of equation (156) is given by

$$\frac{1}{R} \nabla_\Theta \cdot S = \frac{\mu_r \mu_o}{R_I Y} \left(\nabla_\Theta \cdot \hat{S} \right), \qquad (162)$$

where $\hat{S}$ represents the nondimensionalised First Piola Kirchoff stress and $\mu_r = \mu/\mu_o$. Equating equations (161) and (162) results in the linearised, nondimensionalised polar component for the collapse phase of the linear momentum which is

$$Y^2 \epsilon \left(\frac{\partial^2 h}{\partial \hat{t}^2} \right) e_\theta = \mu_r \nabla_\Theta \cdot \hat{S} \qquad (163)$$

where $\gamma = \sqrt{\rho_o R_I^2 / \mu_o}$. The nondimensionalised polar component of the First Piola Kirchoff stress $\hat{S}$ for the collapse phase of the shell is related to the quasistatic equation represented by equations (105) and (113). In the collapse phase each contributing term in equation (113) will contribute a negative stress value which represents a compression whilst the perturbation in the collapse phase is denoted by $\epsilon h(\Theta, \hat{t})$ rather than $\epsilon g(\Theta)$ for the quasistatic (forward) picture. Adjusting the signs in equation (113) such that all the terms are negative in magnitude and applying the appropriate time evolving perturbation $\epsilon h(\Theta, \hat{t})$ results in a nondimensionalised polar stress term given by

$$\nabla_\Theta \cdot \hat{S} = \epsilon \mu_r \left(-2\beta |h''| - 2\beta |h' \cot \Theta| - 2\beta h \csc^2 \Theta \right) e_\theta, \qquad (164)$$

42

which leads to the polar component of the linear momentum

$$Y^2 \frac{\partial^2 h}{\partial \hat{t}^2} = \mu_r \left(-2\beta |h''| - 2\beta |h' \cot \Theta| - 2\beta h \csc^2 \Theta \right). \tag{165}$$

The polar component of the linear momentum represented by equation (165) is solved numerically using finite differences. To solve equation (165) we require two boundary and two initial conditions. The boundary condition at the opening angle Θ_{op} is such that $\hat{\tau}_{\theta\theta} \left(\Theta_{op}, \hat{t} \right) = 0$ which leads to

$$h' + h \cot \Theta_{op} = 0, \tag{166}$$

and at the matching boundary condition

$$h(\Theta_s, \hat{t}) = 0. \tag{167}$$

The initial conditions are

$$h(\Theta, 0) = g(\Theta), \tag{168}$$

$$\text{and } \frac{\partial h(\Theta, 0)}{\partial \hat{t}} = 0, \tag{169}$$

where equation (168) sets $h(\Theta, \hat{t})$ for the angular collapse phase at $\hat{t} = 0$ equal to the forward picture $g(\Theta)$. This implies that there is no hysteresis in the collapse phase of the shell and that the forward and collapse paths are identical. This is a consequence of there being no viscoelasticity in the physical model.

43

14 Results for the deformation of an open shelled spherical microbubble
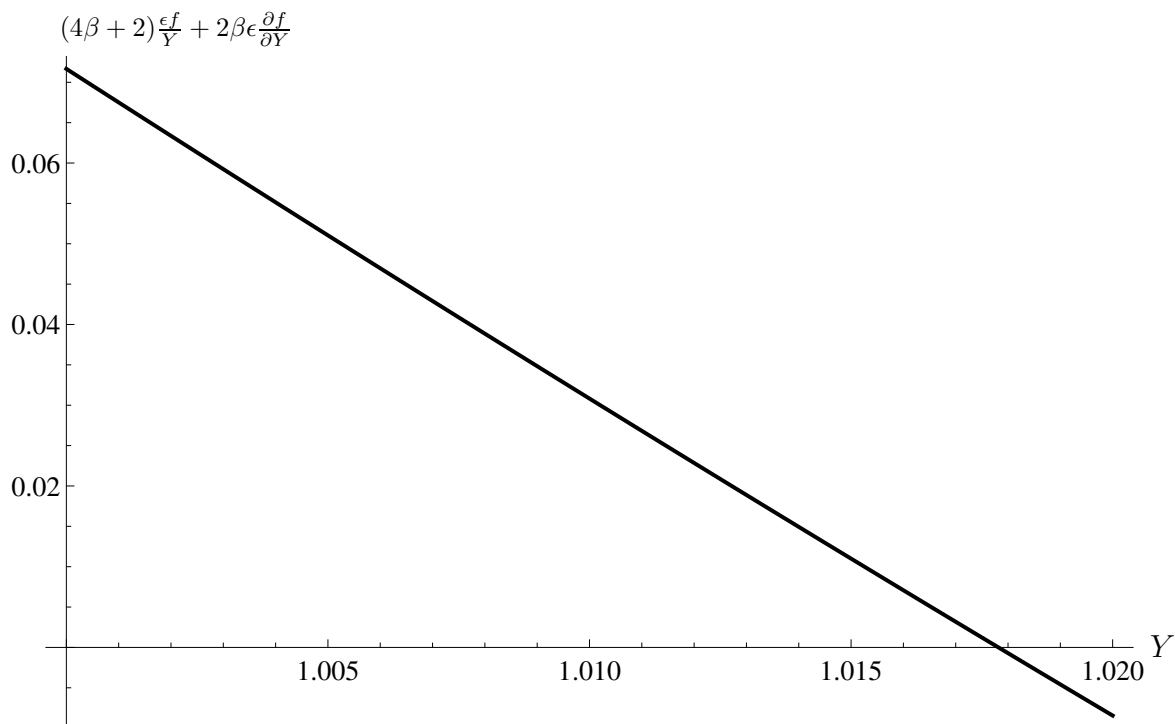
Figure 3: Graph of the radial terms in the polar hoop stress boundary condition for equation (112) for $\beta = 24.5$.

Figure 3 highlights how the magnitude of the radial terms in equation (112) vary with Y and illustrates that the contribution of $(4\beta + 2)\epsilon f/Y + 2\beta\epsilon\partial f/\partial Y$ to the nondimensionalised boundary condition is small. This justifies neglecting the radial terms in equation (112) which results in an angular boundary condition that is independent of Y.
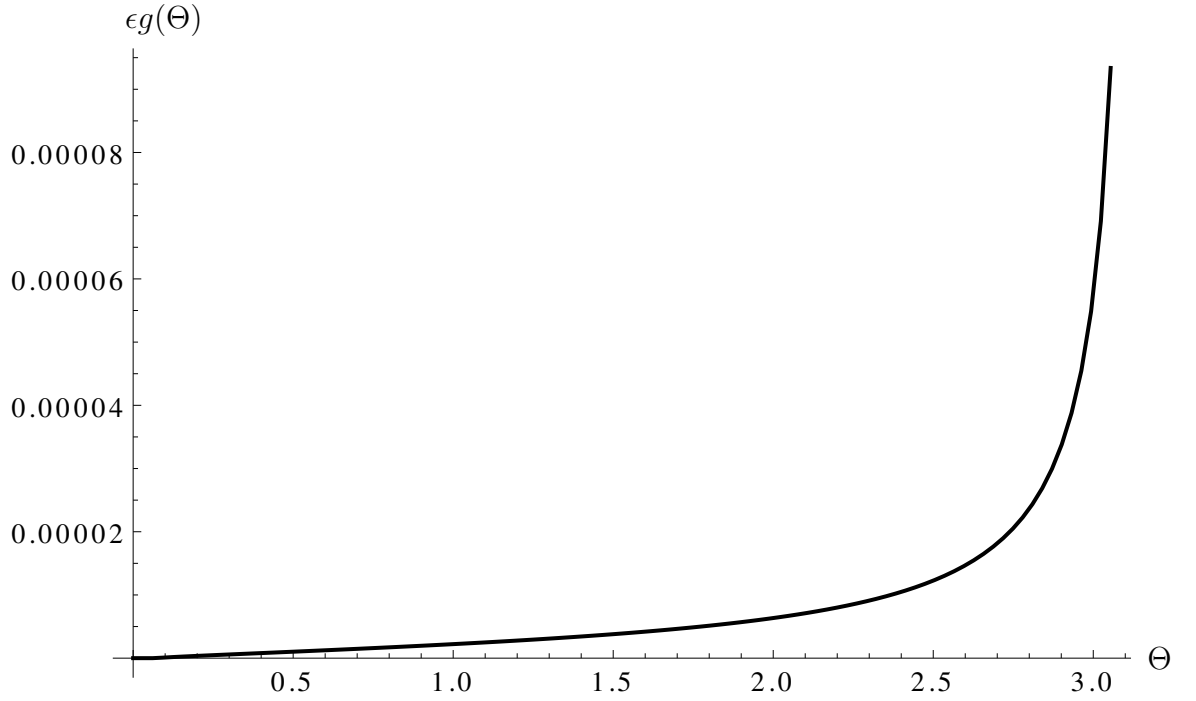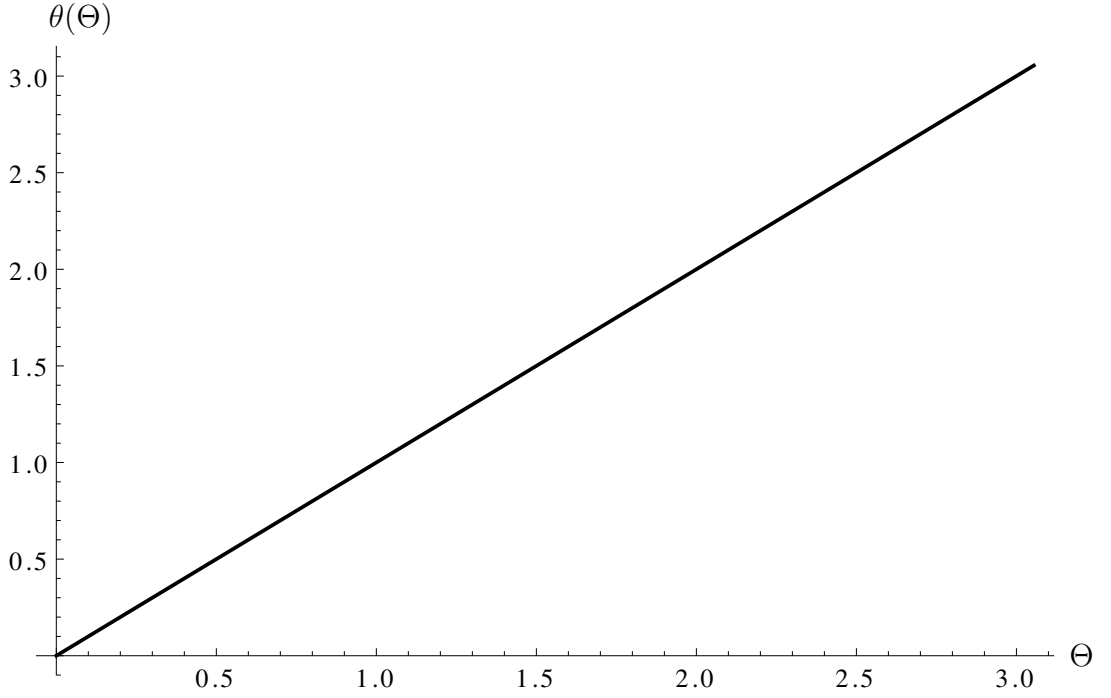
Figure 4: Graph of the angular perturbation for an open shell versus the reference angle for a nondimensionalised hoop stress load of $\hat{p} = 0.0002$ where $\mu = 20\text{MPa}$, $\nu = 0.49$, $\beta = 24.5$ and an initial thickness of $Y_O - Y_I = 0.02$ for an opening angle of $\pi - \Theta_{op} = \pi/36$ and a matching boundary condition given at $\Theta_s = \pi/45$. This is calculated using equation (118).

Figure 4 illustrates how the angular perturbation, $\epsilon g(\theta)$, varies with the polar angle, Θ, in the reference configuration for a small opening angle $\pi - \Theta_{op} = \pi/36$ and a nondimensionalised stress of $\hat{p} = 0.0002$. $\epsilon g(\theta)$, the perturbation of $\theta(\Theta)$, is nonlinear and small in magnitude which is a consequence of the small opening angle, $\pi - \Theta_{op}$.

Figure 5: Graph of $\theta(\Theta)$ for an open shell versus the reference angle, Θ, for a nondimensionalised stress load of $\hat{p} = 0.0002$ where $\mu = 20\text{MPa}$, $\nu = 0.49$, $\beta = 24.5$ and an initial thickness of $Y_O - Y_I = 0.02$ for an opening angle of $\pi - \Theta_{op} = \pi/36$ and a matching boundary condition at $\Theta_s = \pi/45$. This is calculated using equation (118).

Figure 5 highlights how the polar angle, $\theta(\Theta)$, in the current configuration varies with the polar angle in the reference configuration, Θ, for a small opening angle given by $\pi - \Theta_{op} = \pi/36$ and a matching boundary condition applied to the vicinity of the north pole at $\Theta_s = \pi/45$. The polar angle $\theta(\Theta)$ is linear in nature due to the small perturbation in $\epsilon g(\theta)$ which is a result of the small opening angle $\pi - \Theta_{op}$. At the polar angular region of $0 \leq \Theta \leq \pi/45$ the angular perturbation is $\epsilon g(\theta) = 0$ and $\theta(\Theta) = \Theta$. This region represents the purely radially compressive region of the sphere where the matching boundary condition is applied in the vicinity of the north pole in order to avoid a coordinate singularity in the Jacobian, J, given by equation (14).
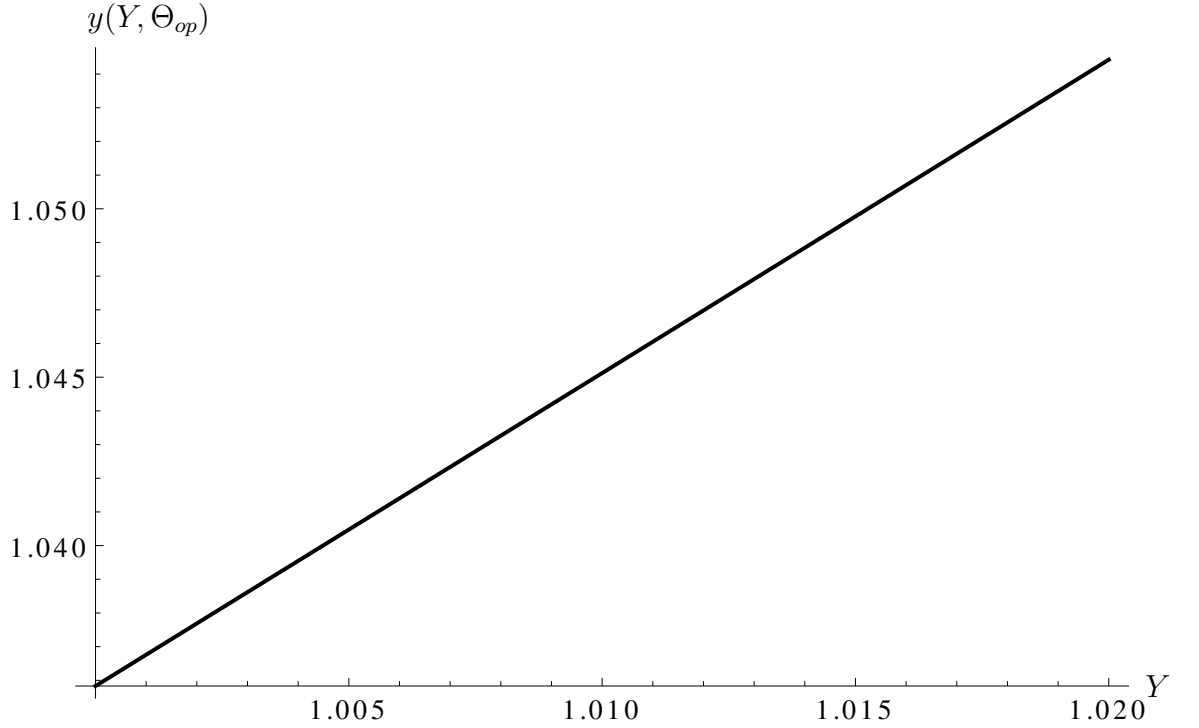
46

Figure 6: Graph of the nondimensionalised radius in the current configuration $y(Y, \Theta)$ versus the nondimensionalised radius in the reference configuration Y for a nondimensionalised stress load $\hat{p} = 0.0002$ where $\mu = 20$MPa, $\nu = 0.49$, $\beta = 24.5$ and an initial thickness of $Y_O - Y_I = 0.02$ for an opening angle of $\pi - \Theta_{op} = \pi/36$ and a matching boundary condition at $\Theta_s = \pi/45$. This is calculated using equations (122) and (129).

Figure 6 illlustrates the linear relationship between the radius $y(Y, \Theta_{op})$ in the current configuration and the radius in the reference configuration, Y, for a small opening angle $\pi - \Theta_{op} = \pi/36$ and a nondimensionalised stress $\hat{p} = 0.0002$. Note that the $y(Y, \Theta_{op})$ is larger than Y indicating that the shell has been displaced outwards by a very small amount.
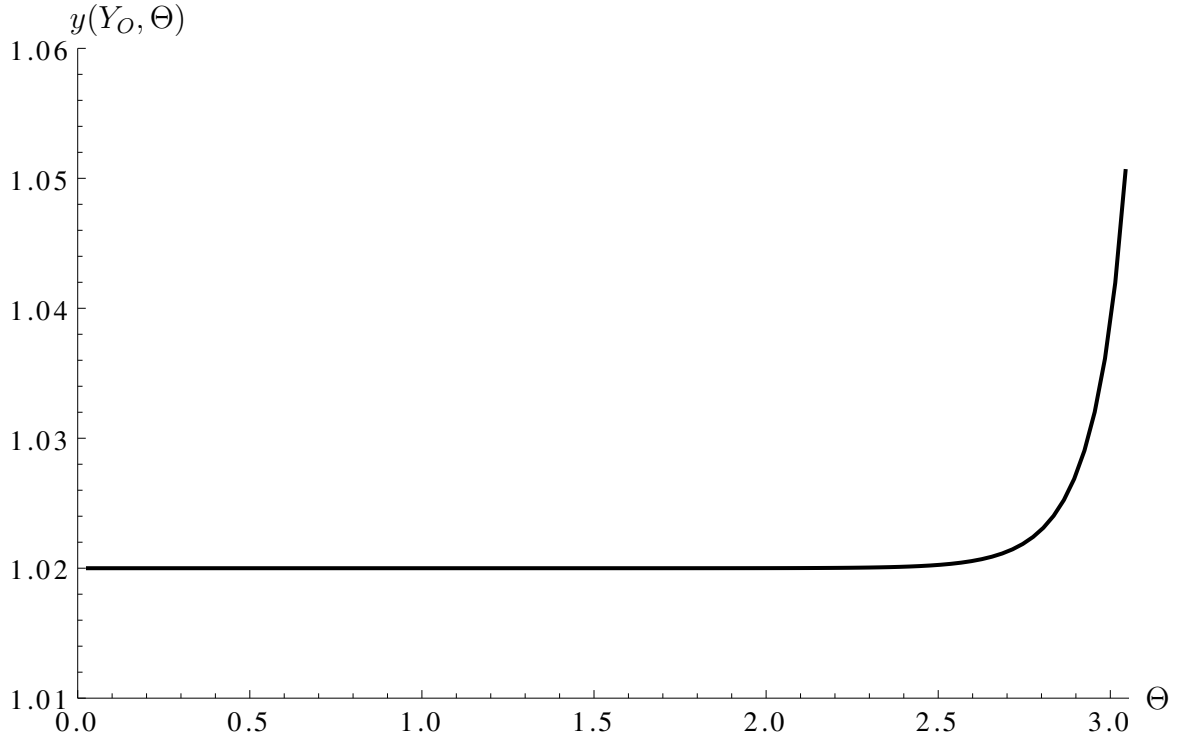
Figure 7: Graph of the nondimensionalised radius in the current configuration $y(Y, \Theta)$ versus Θ for a nondimensionalised stress load $\hat{p} = 0.0002$ where $\mu = 20$MPa, $\nu = 0.49$, $\beta = 24.5$ and an initial thickness of $Y_O - Y_I = 0.02$ for an opening angle of $\pi - \Theta_{op} = \pi/36$ and a matching boundary condition at $\Theta_s = \pi/45$. This is calculated using equations (122) and (129).

Figure 7 illustrates the nonlinear relationship between the radius $y(Y_O, \Theta)$ in the current configuration and the reference angle Θ for a small opening angle $\pi - \Theta_{op} = \pi/36$ and a nondimensionalised stress $\hat{p} = 0.0002$ evaluated at Y_O. As Θ approaches Θ_{op} there is a nonlinear growth in $y(Y_O, \Theta)$.
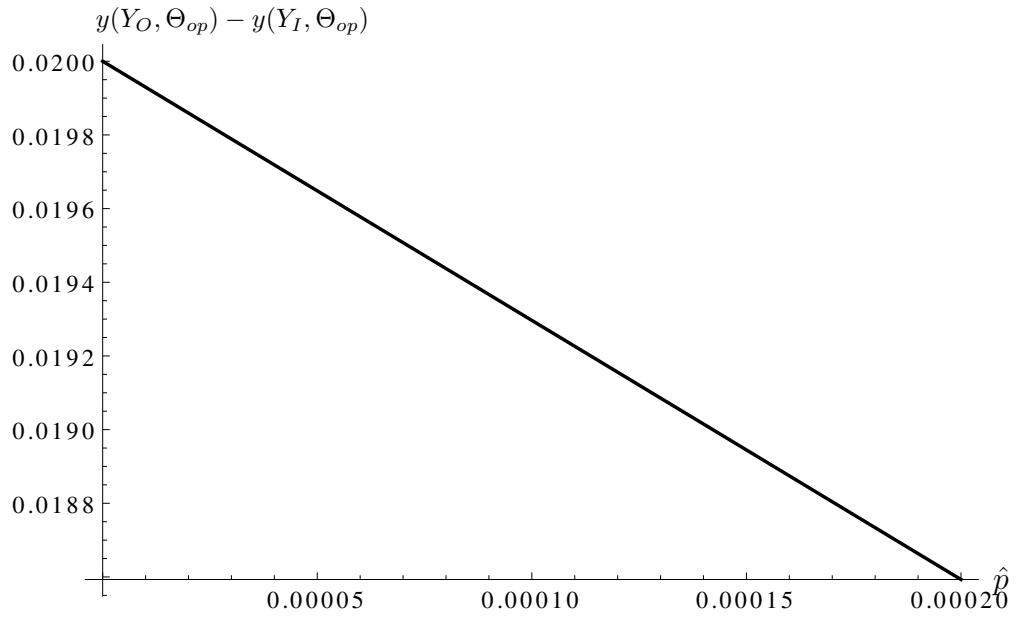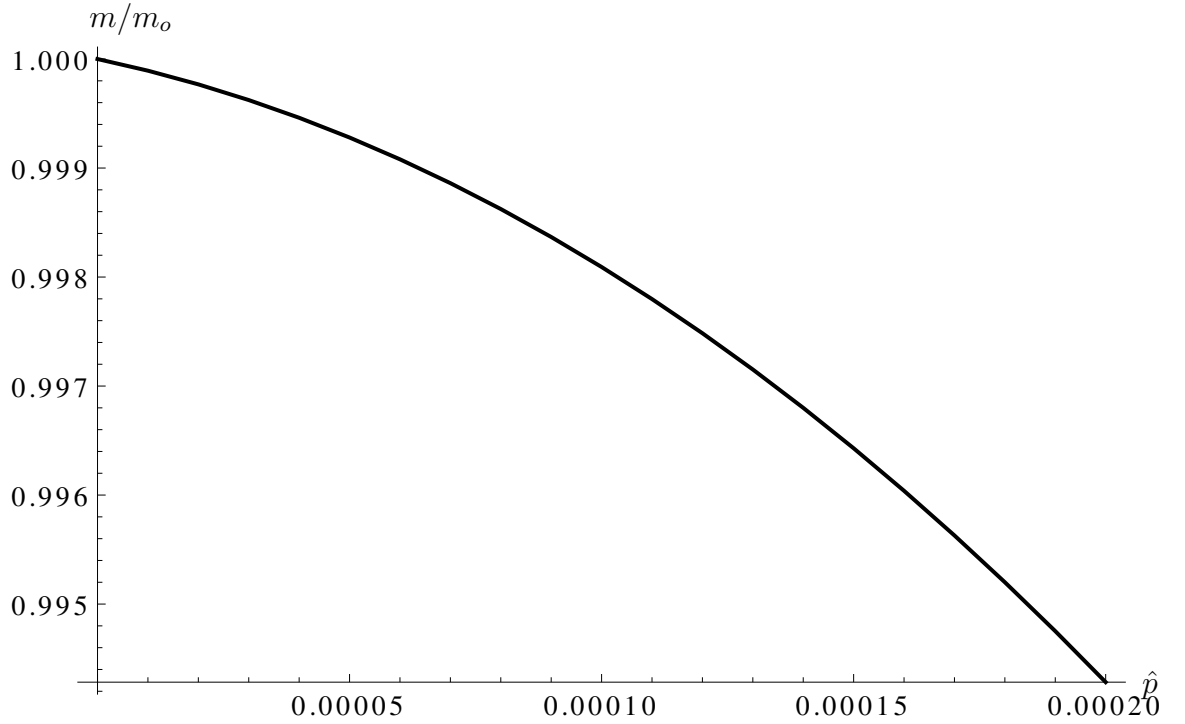
Figure 8: Graph of the Jacobian for a series of nondimensionalised stresses loads up to $\hat{p}$ = 0.0002 where μ = 20MPa, ν = 0.49, β = 24.5 and an initial thickness of $Y_O - Y_I = 0.02$ for an opening angle of $\pi - \Theta_{op} = \pi/36$ and a matching boundary condition at $\Theta_s = \pi/45$. This is calculated using equations (122) and (129).

Figure 8 shows how the thickness of the shell $y(Y_O, \Theta_{op}) - y(Y_I, \Theta_{op})$ thins down as a series of applied nondimensionalised stresses $\hat{p}$ up to $\hat{p} = 0.0002$ are applied to the rim of the shell.

Figure 9: Graph of the normalised mass m/m_o for a series of nondimensionalised stresses loads up to $\hat{p} = 0.0002$ where $\mu = 20\text{MPa}$, $\nu = 0.49$, $\beta = 24.5$ and an initial thickness of $Y_O - Y_I = 0.02$ for an opening angle of $\pi - \Theta_{op} = \pi/36$ and a matching boundary condition at $\Theta_s = \pi/45$. This is calculated using equations (74), (122) and (129).

Figure 9 illustrates how the normalised mass of a stressed shell evolves (forward picture) over a range of nondimensionalised stresses $\hat{p}$ up to $\hat{p} = 0.0002$ and highlights that the error in mass conservation is $\approx 0.6\%$.

15 Results for the collapse phase of an open shelled spherical microbubble

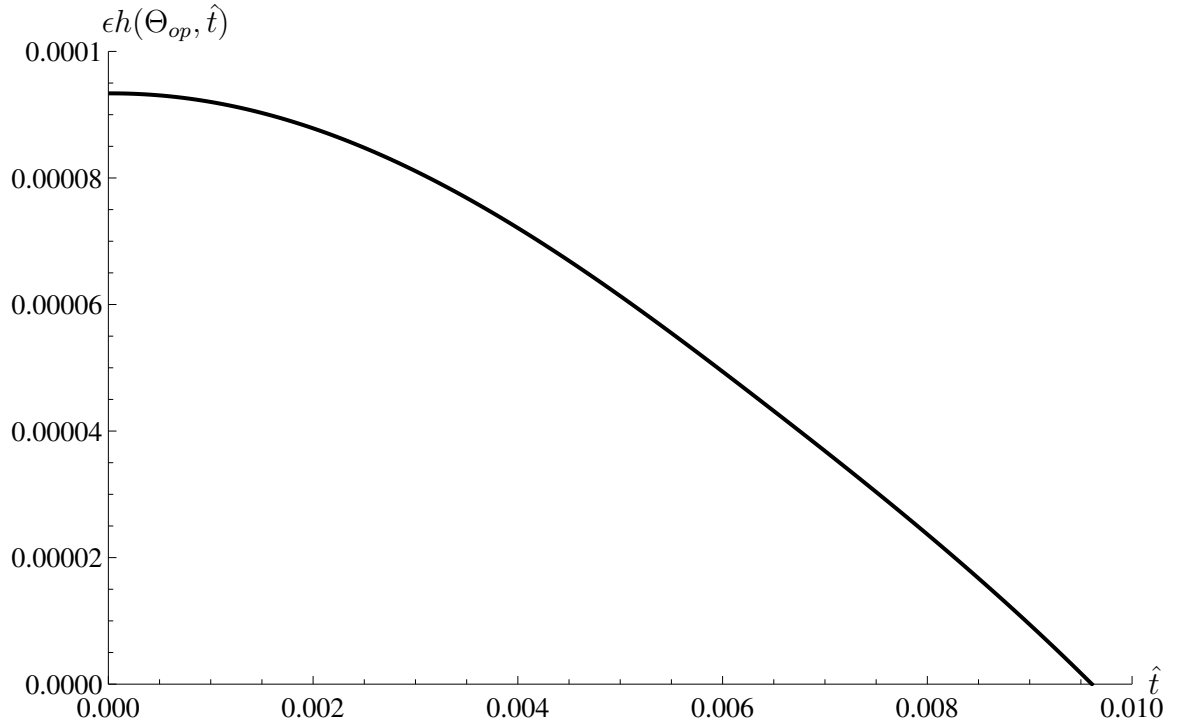THis section will discuss the results for a collapsing shell.

Figure 10: Graph of the polar angle perturbation $h(\Theta_{op}, \hat{t})$ versus the nondimensionalised time for $\mu = 20\text{MPa}$, $\nu = 0.49$, $\beta = 24.5$, an initial thickness of $Y_O - Y_I = 0.02$, an opening angle of $\pi - \Theta_{op} = \pi/36$ and a matching boundary condition at $\Theta_s = \pi/45$. This is calculated using equations (165), (166), (167), (168) and (169).

Figure 10 shows how the polar angle perturbation $\epsilon h(\Theta, \hat{t})$ varies with the nondimensionalised time as the stressed shell collapses back to its original stress free configuration when $\nabla_\theta \cdot \tau = 0$. Figure 10 illustrates that the nonlinear trend is a sinusoidal function described by equation (165) describing simple harmonic motion. This is a consequence of the negative stress (compressive) terms which cause the stressed shell to collapse to its original stress free configuration.
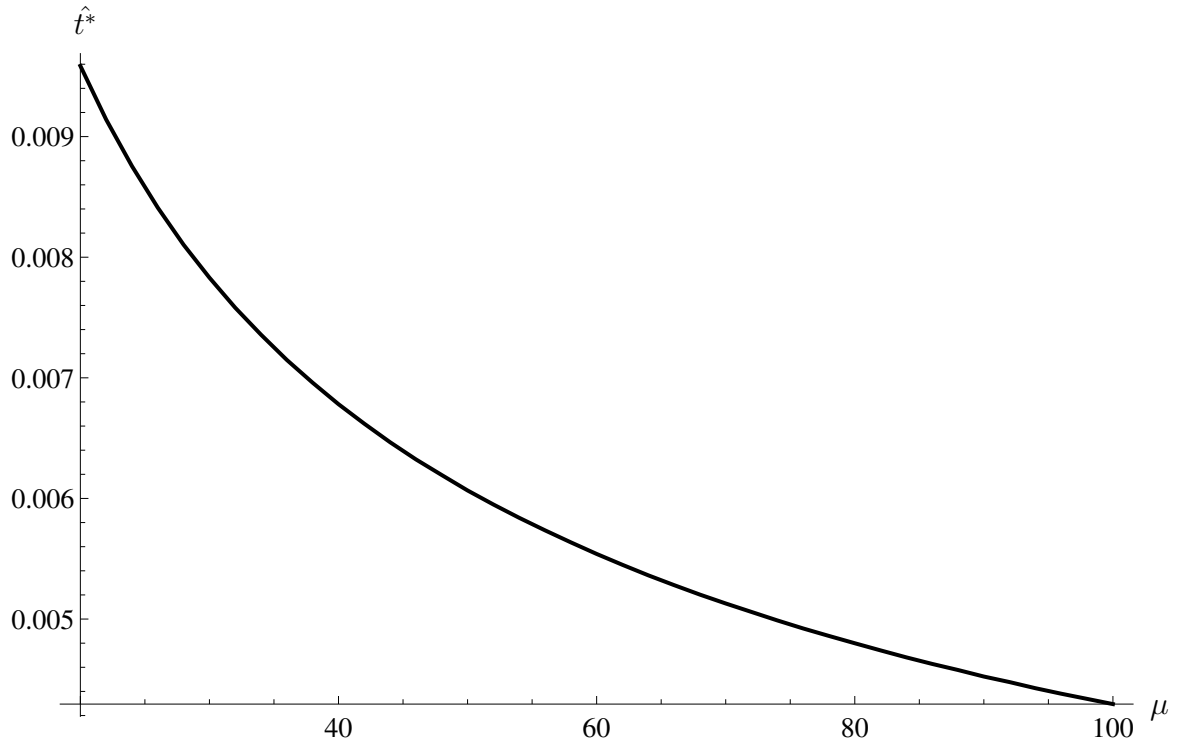
Figure 11: Graph of the nondimensionalised collapse time for the collapse phase of the shell versus a range of shear modulus values for $\nu = 0.49$, $\beta = 24.5$, an initial thickness of $Y_O - Y_I = 0.02$, an opening angle of $\pi - \Theta_{op} = \pi/36$ and a matching boundary condition at $\Theta_s = \pi/45$. This is calculated using equations (165), (166), (167), (168) and (169).

Figure 11 illustrates how the collapse time decreases nonlinearly with an increasing shear modulus. A smaller shear modulus experiences a larger displacement due its lower stiffness. Larger displacements (for a given fixed stress p) will take longer to collapse back to their initial stress free position. Therefore as the shear modulus increases there is a reduction in the shell's displacement which results in faster collapse times.
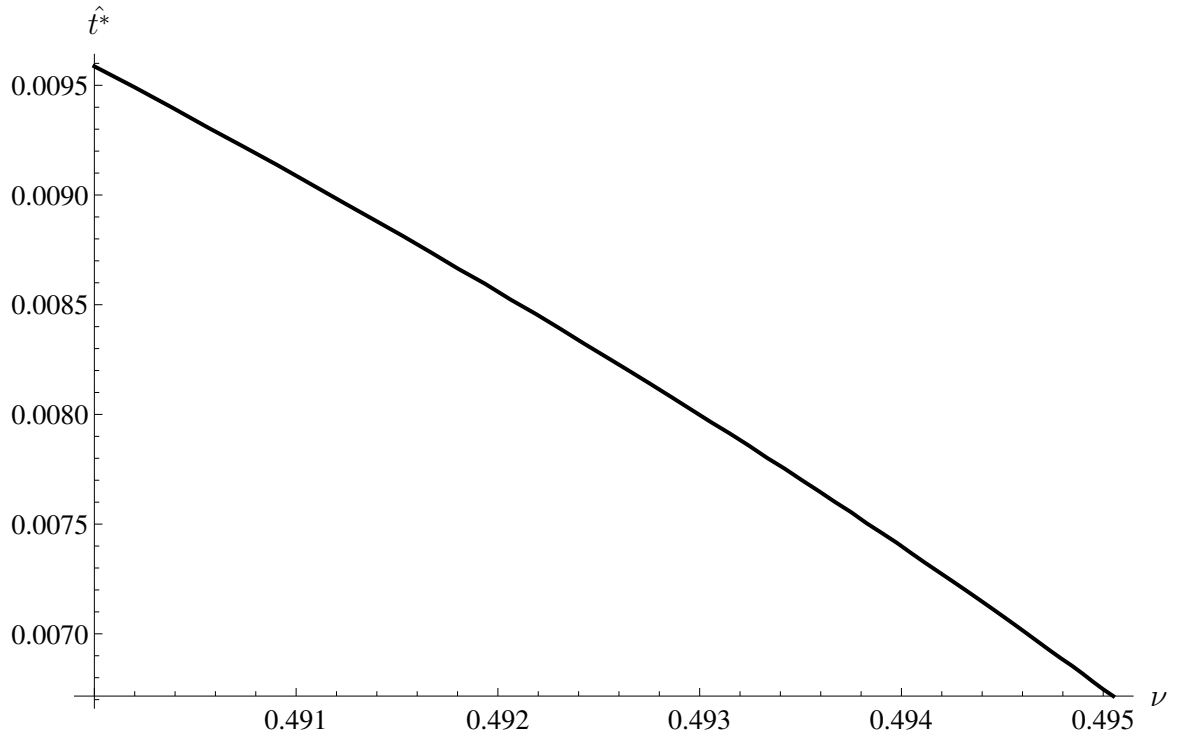
Figure 12: Graph of the nondimensionalised collapse time versus a range of Poisson ratios for $\mu = 20\text{MPa}$, an opening angle of $\pi - \Theta_{op} = \pi/36$ and a matching boundary condition at $\Theta_s = \pi/45$. This is calculated using equations (165), (166), (167), (168) and (169).

Figure 12 shows that when the Poisson ratio, ν, increases then the collapse time of the shell decreases, resulting in a faster collapse time. This relationship is effectively linear in nature and is modelled over the typical range of Poisson values for soft tissue, namely $\nu = 0.49$ to 0.495. This trend arises because smaller Poisson ratios experience larger displacements which results in longer, slower collapse times.
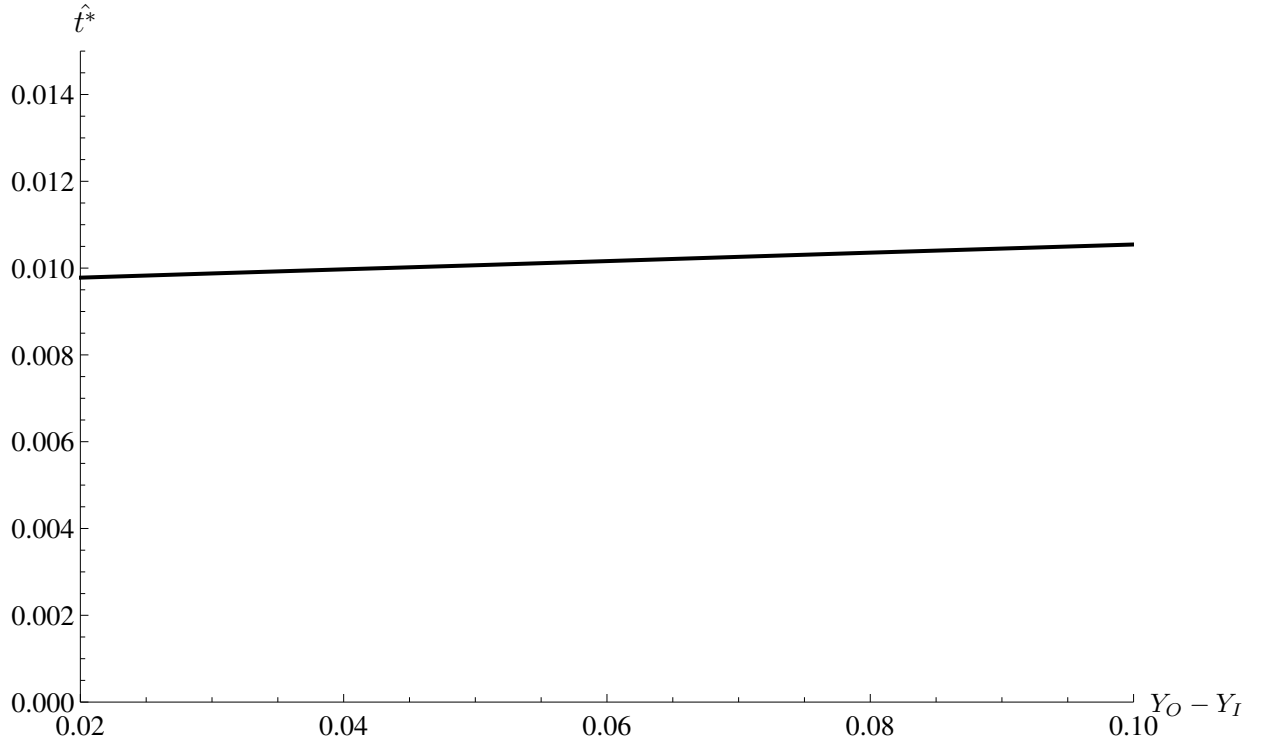
Figure 13: Graph of the nondimensionalised collapse time $\hat{t}^*$ versus a range of nondimensionalised stress free shell thicknesses ranging from $Y_O - Y_I = 0.02$ to 0.10 for $\mu = 20\text{MPa}$, $\nu = 0.49$, $\beta = 24.5$, an opening angle of $\pi - \Theta_{op} = \pi/36$ and a matching boundary condition at $\Theta_s = \pi/45$. This is calculated using equations (165), (166), (167), (168) and (169).

Figure 13 highlights how the collapse time slightly increases linearly with varying shell thicknesses (reference configuration thickness). Generally thinner shell require a lower applied stress to create a particular angular displacement, hence the resulting tensions are lower, and a higher collapse time results. However, careful analysis of equation (165) reveals a dependency on Y^2. Thus as the thickness of the shell increases the acceleration downwards during the collapse phase of the shell is reduced by a factor of $1/Y_O^2$ resulting in a longer collapse time.
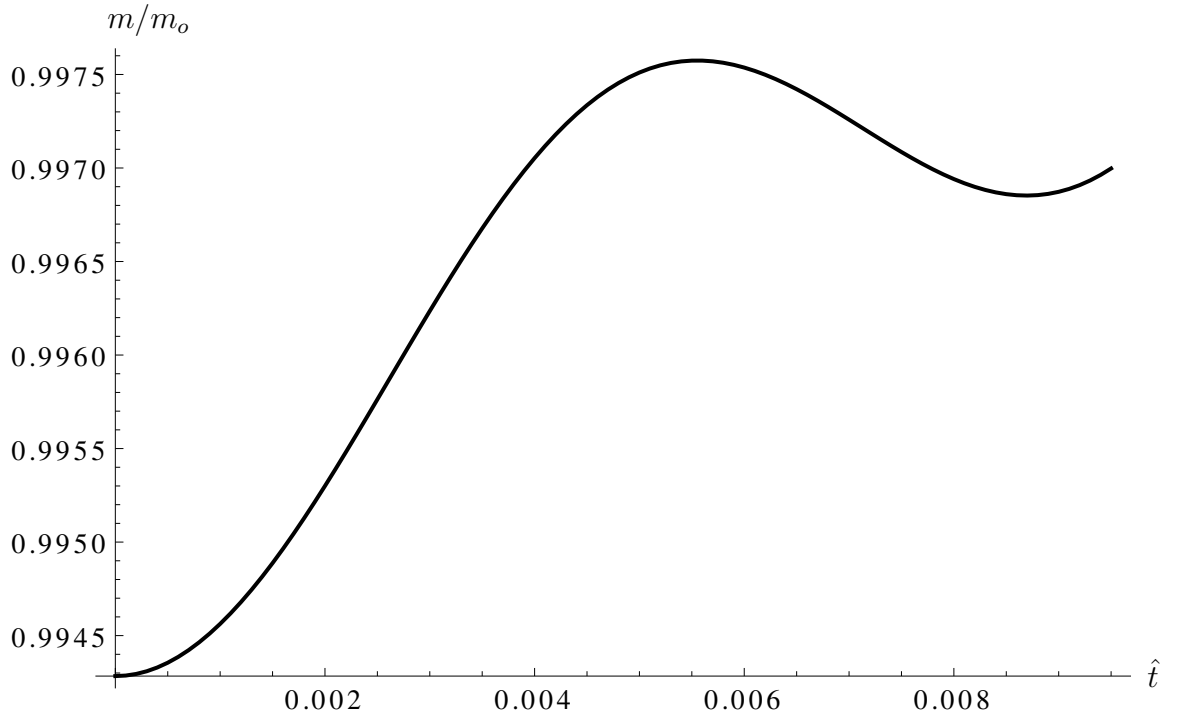
Figure 14: Graph of the normalised mass m/m_o of a stressed, collapsing shell where $\mu = 20\text{MPa}$, $\nu = 0.49$, $\beta = 24.5$ and an initial thickness of $Y_O - Y_I = 0.02$ for an opening angle of $\pi - \Theta_{op} = \pi/36$ and a matching boundary condition at $\Theta_s = \pi/45$. This is calculated using equations (165) to (169).

Figure 14 illustrates that the normalised mass of a collapsing shell versus the nondimensionalised time is nonlinear in nature. The error in mass conservation is $\approx 0.3\%$.
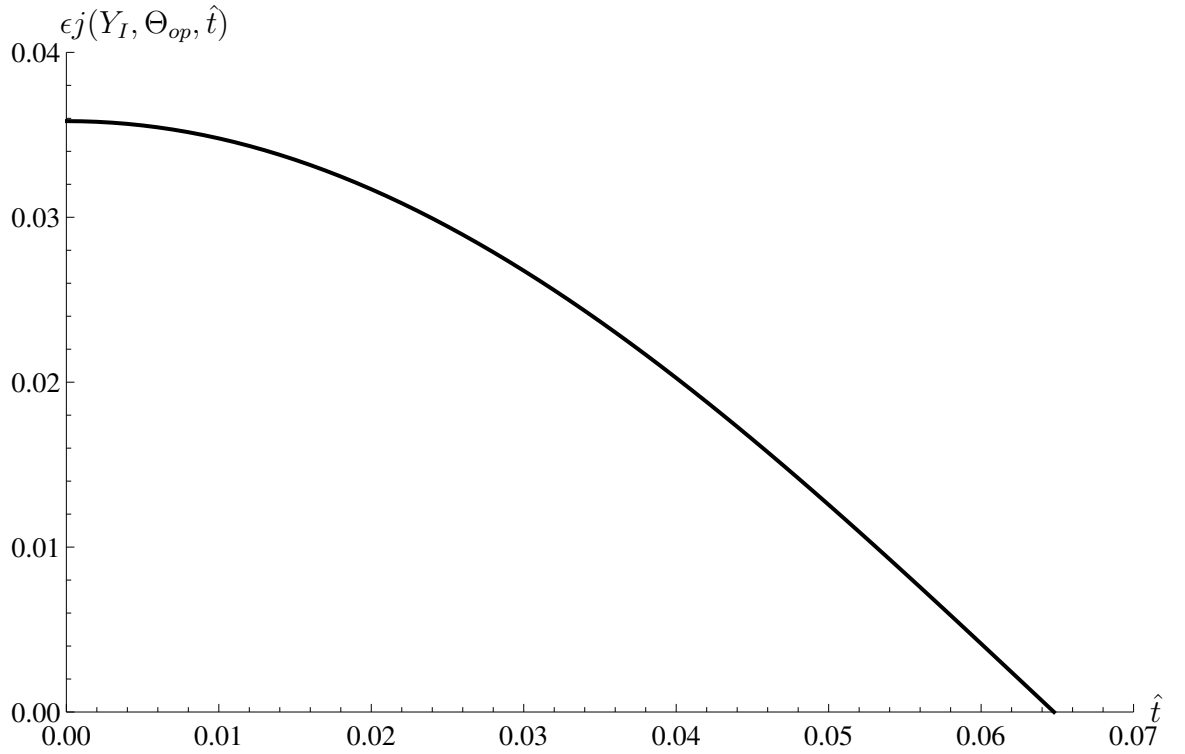
Figure 15: Graph of the radial perturbation $j(Y_I, \Theta_{op}, \hat{t})$ versus the nondimensionalised time for $\mu = 20\text{MPa}$, $\nu = 0.49$, $\beta = 24.5$, an initial thickness of $Y_O - Y_I = 0.02$, an opening angle of $\pi - \Theta_{op} = \pi/36$ and a matching boundary condition at $\Theta_s = \pi/45$. This is calculated using equations (142), (144), (145), (151) and (155).

Figure 15 shows how the radial perturbation $\epsilon j(Y_I, \Theta_{op}, \hat{t})$ varies with the nondimensionalised time as the stressed shell collapses back to its original stress free configuration when $\nabla_y \cdot \tau = 0$. Figure 15 illustrates that the nonlinear trend is a sinusoidal function that is characterised as simple harmonic motion. This is a consequence of the negative stress (compressive) terms which cause the stressed shell to collapse to its original stress free configuration. Note that the radial collapse time is $\hat{t}^* \approx 0.09$ and is slower than the polar angular collapse. We would expect both the radial and polar collapses to be simultaneous with the exact same collapse times. This difference in collapse times may be due to the various approx-

56

imations that have been made when performing the linearisation process. For the radial displacement the collapse times and their dependency on varying material parameters display similar characteristic trends as Figures 11, 12 and 13.

16   Experimental v theoretical results

This section compares the theoretical model with published experimental results. The Müller experiment [7] illustrates how the collapsing shelled millibubble's displacement varies linearly with time. This linear relationship allows us to extrapolate Müller's experimental results and also supports the use of linearisation for the analytical model. The theoretical model for the open shelled collapse was compared to the Müller experiment [7]. The shear modulus of the shell was taken as $\mu = 20$MPa with a density of $\rho = 1100 kgm^{-3}$ [17]. A 4.5mm stressed shelled millibubble of thickness 1460nm with a Poisson ratio of $\nu = 0.49$ has a theoretical collapse time of $t^* = 3.2 \times 10^{-7}$s whereas the experimental result from Müller was found to be $t^* = 7.4 \times 10^{-7}$s. There are various reasons as to why the theoretical model's collapse time differs from the experimentally observed value. The material parameters used for the theoretical model may not exactly match the experimental values in [7]. The strain energy density function used in this study may not accurately describe the smectic A dynamics.

17   Conclusion

This study has focussed on how the material parameters such as the shear modulus, Poisson's ratio and the shells equilibrium (stress free) thickness influences the collapse time of a stressed shell as the shell collapses from its stressed configuration back to its original stress free configuration. An opening angle was used to model

the stress free configuration with a polar hoop stress being applied to deform both radially and angularly the open sphere. The Cauchy polar hoop stress was then set to zero causing the stressed shell to collapse to its stress free configuration. This collapse phase was timed by applying the conservation of mass and energy and by assuming that there was no viscosity or viscoelastic effects in the model that would lead to hysteresis. A typical shell with an opening angle of $\pi - \Theta_{op} = \pi/36$, a nondimensionalised stress free thickness of $Y_O - Y_I = 0.02$, a nondimensionalised shear modulus of $\mu = 20\text{MPa}$ and a typical soft tissue Poisson ratio of $\nu = 0.49$ has a nondimensionalised collapse time of $\hat{t^*} = 0.0096$. As the shear modulus increases the collapse time decreases in a nonlinear manner. Thicker shells have slightly longer collapse times which is a consequence of the shells possessing a smaller acceleration towards their equilibrium position. Smaller Poisson ratios have longer, slower collapse times with the relationship between the collapse time and Poisson's ratio being effectively linear in nature. The theoretical model compares well with published experimental results for smectic A millibubbles [7]. A theoretical collapse time of $t^* = 3.2 \times 10^{-7}$s was determined whereas the published experimental result from Müller was found to be $t^* = 7.4 \times 10^{-7}$s.

References

[1] E. Stride and N. Saffari. Microbubble ultrasound contrast agents: a review. *Proceedings of the Institution of Mechanical Engineers Part H*, 217:429–447, 2003.

[2] J. McLaughlan, N. Ingram, P.R. Smith, S. Harput, P.L. Coletta, S. Evans, and S. Freear. Increasing the sonoporation efficiency of targeted polydisperse

microbubble populations using chirp excitation. *IEEE Transactions on ultrasonics, Ferroelectrics and frequency control*, 60:2511–2520, 2013.

[3] O. Falou, A.J. Sojahrood, J.C. Kumaradas, and M.C. Kolios. Modelling the effect of shell thickness on high frequency ultrasound scattering from ultrasound contrast agents. *Canadian Acoustics*, 38:38–39, 2010.

[4] G. A. Sotiriou, F. Starsich, A. Dasargyri, M. C. Wurnig, F. Krumeich, A. Boss, Jean-Christophe Leroux, and S. E. Pratsinis. Photothermal killing of cancer cells by the controlled plasmonic coupling of Silica-coated Au/Fe_2O_3 nanoaggregates. *Advanced Functional Materials*, 24:2818–2827, 2014.

[5] M.J.K. Blomley, J.C. Cooke, E.C. Unger, M.J. Monaghan, and D.O. Cosgrove. Microbubble contrast agents: a new era in ultrasound. *British Medical Journal*, 322:1222–1225, 2001.

[6] Lord Rayleigh. On the pressure developed in a liquid during the collapse of a spherical bubble. *Philosophical Magazine, Series 6*, 34:94–98, 1917.

[7] F. Müller and R. Stannarius. Comparison of the rupture dynamics of smectic bubbles and soap bubbles. *Liquid Crystals*, 36:133–145, 2009.

[8] V.A. Bogoyavlenskiy. Differential criterion of a bubble collapse in viscous liquids. *Physical Review E*, 60:504–508, 1999.

[9] K. Tsiglifis and N.A. Pelekasis. Nonlinear radial oscillations of encapsulated microbubbles subject to ultrasound: The effect of membrane constitutive law. *Journal Acoustical Society of America*, 123:4059–4070, 2008.

[10] K.A. Lazopoulos and R.W. Ogden. Spherically symmetric solutions for a spherical shell in finite pseudo-elasticity. *European Journal of Mechanics - A/Solids*, 18:617–632, 1999.

[11] A.A. Doinikov and A. Bouakaz. Review of shell models for contrast agent microbubbles. *IEEE Transactions on Ultrasonics, Ferroelectrics and Frequency Control*, 58:981–993, 2011.

[12] Y. Gorb and J.R. Walton. Dependence of the frequency spectrum of small amplitude vibrations superimposed on finite deformations of a nonlinear, cylindrical elastic body on residual stress. *International Journal of Engineering Science*, 48:1289–1312, 2010.

[13] R.W. Ogden. *Nonlinear Elastic Deformations*. Dover, New York, 1997.

[14] G.A. Holzapfel. *Nonlinear Solid Mechanics*. Wiley, Wiltshire, 2000.

[15] K. Gou, S. Joshi, and J.R. Walton. Recovery of material parameters of soft hyperelastic tissue by an inverse spectral technique. *International Journal of Engineering Science*, 56:1–16, 2012.

[16] D. J. Acheson. *Elementary Fluid Dynamics*. Oxford University Press, New York, 1990.

[17] J. Tu, J. Guan, Y. Qiu, and T.J. Matula. Estimating the shell parameters of sonovue microbubbles using light scattering. *Journal Acoustical Society of America*, 126:2954–2962, 2009.